
Article:
van der Sluijs, R.V., Verkennis, A.E.E., Hodskinson, M.R. et al. (17 more authors) (2025) DNA polymerase kappa is the primary translesion synthesis polymerase for aldehyde ICLs. Nucleic Acids Research, 53 (18). gkaf875. ISSN: 0305-1048

https://doi.org/10.1093/nar/gkaf875

Nucleic Acids Research, 2025, **53**, gkaf875
https://doi.org/10.1093/nar/gkaf875
Genome integrity, repair and replication

DNA polymerase kappa is the primary translesion synthesis polymerase for aldehyde ICLs

Roxanne V. van der Sluijs[1,2,3], Alexander E.E. Verkennis[1,2,3], Michael R. Hodskinson[4], Jamie Barnett[1,2,3], Victoria M. Cruz[1,2,3,5], Miguel Hernandez-Quiles[1,6], Themistoklis Liolios[1,2,3], Sally B. Morton[7,8], Aiko Hendrikx[1,2], Collin Bos[1,2,3], Harm Post[9,10], Christopher L. Millington[4,11], Clément Rouillon[2,12], Giulia Ricci[2], Francesca Mattiroli[2], David M. Williams[7], Maarten Altelaar[9,10], Michiel Vermeulen[1,6,13], K.J. Patel[4,11], Puck Knipscheer[1,2,3,*]

[1]Oncode Institute, 3521 AL Utrecht, The Netherlands
[2]Hubrecht Institute-KNAW and University Medical Center Utrecht, 3584 CT Utrecht, The Netherlands
[3]Department of Human Genetics, Leiden University Medical Center, 2333 ZG Leiden, The Netherlands
[4]MRC Laboratory of Molecular Biology, Cambridge CB2 0QH, United Kingdom
[5]Present address: The Princess Máxima Center for Pediatric Oncology, 3584 CS Utrecht, The Netherlands
[6]Division of Molecular Genetics, Netherlands Cancer Institute, 1066 CX Amsterdam, The Netherlands
[7]Sheffield Institute for Nucleic Acids, School of Mathematical and Physical Sciences, University of Sheffield, Brook Hill, Sheffield S3 7HF, United Kingdom
[8]Present address: Doncaster Royal Infirmary, Clinical Laboratory Sciences, Armthorpe Road, Doncaster DN2 5LT, United Kingdom
[9]Biomolecular Mass Spectrometry and Proteomics, Bijvoet Center for Biomolecular Research and Utrecht Institute for Pharmaceutical Sciences, University of Utrecht, 3584 CH Utrecht, The Netherlands
[10]Netherlands Proteomics Center, 3584 CH Utrecht, The Netherlands
[11]Present address: MRC Weatherall Institute of Molecular Medicine, University of Oxford, John Radcliffe Hospital, Oxford OX3 9DS, United Kingdom
[12]Present address: Division of Cell Biology, The Netherlands Cancer Institute, 1066 CX Amsterdam, The Netherlands
[13]Department of Molecular Biology, Faculty of Science, Radboud Institute for Molecular Life Sciences, Radboud University, 6525 GA Nijmegen, The Netherlands

*To whom correspondence should be addressed. Email: p.knipscheer@hubrecht.eu

Abstract

DNA interstrand crosslinks (ICLs) are highly cytotoxic lesions that block essential cellular processes like replication and transcription. Endogenous ICLs can be induced by reactive aldehydes produced during normal cellular metabolism. Defective repair of these aldehyde-induced ICLs is associated with Fanconi anaemia (FA), a cancer predisposition syndrome. We previously showed that acetaldehyde-induced ICLs are repaired by the FA pathway and a novel excision-independent pathway. Here, we demonstrate that ICLs induced by acrolein, another cellular aldehyde, are also repaired by both pathways, establishing the generality of aldehyde ICL repair. Focusing on the FA pathway, we identify DNA polymerase kappa (Polκ) as the primary translesion synthesis (TLS) polymerase responsible for the insertion step during lesion bypass of unhooked aldehyde ICLs. This function requires Polκ's catalytic activity and PCNA interaction domains but is independent of Rev1 interaction. In contrast, Polκ has a non-catalytic role in the extension step of cisplatin ICL repair that is dependent on Rev1 interaction. Our work reveals a key role for Polκ in aldehyde ICL repair and provides mechanistic insights into how different ICL structures determine the choice of TLS polymerases during repair.

Graphical abstract

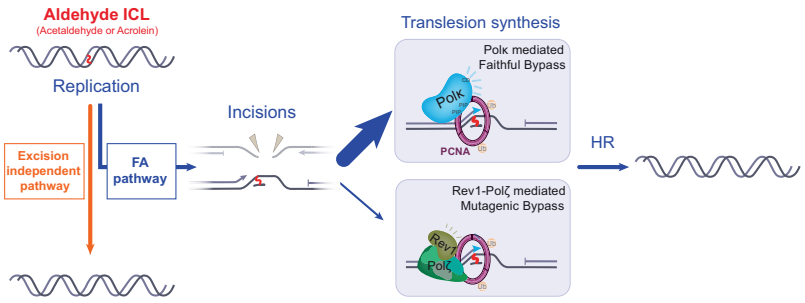

Received: March 31, 2025. **Revised:** July 26, 2025. **Accepted:** July 30, 2025

Introduction

DNA interstrand crosslinks (ICLs) covalently link Watson and Crick DNA strands, preventing their unwinding, which is required for DNA replication and transcription. These highly cytotoxic DNA lesions are exploited in cancer chemotherapy with crosslinking agents but are also induced by endogenous cellular metabolites. An impaired ability to repair ICLs is associated with Fanconi anaemia (FA), a clinically heterogeneous disease characterized by bone marrow failure and a predisposition to cancer. FA results from mutations in one of the currently known 23 FA genes, encoding proteins (FANCA-Y) that act together in the FA pathway to repair ICLs [1–4]. This pathway can resolve ICLs induced by crosslinking agents such as cisplatin, but also those induced by endogenous reactive aldehydes [5–12]. During FA pathway-mediated ICL repair, two DNA replication forks converging at the ICL promote endonucleolytic backbone incisions on one of the DNA strands. This unhooks the crosslink, leaving an ICL adduct on one strand and a double-stranded break (DSB) on the other strand [13–15]. Translesion Synthesis (TLS) bypasses the adducted strand, creating a template for homologous recombination (HR) to resolve the DSB on the other strand [14, 16–18].

Recently, we reported that acetaldehyde-induced ICLs (AA-ICLs) are repaired by the FA pathway but also by a different excision-independent pathway [19]. ICL unhooking in this alternative pathway does not occur via DNA backbone incisions but involves cleavage within the ICL, leaving an adduct that is subsequently bypassed by TLS. However, many mechanistic details of this pathway are still unknown. While the excision-independent repair route is more prone to point mutations than the FA pathway, it is faster and likely reduces the risk of large chromosomal rearrangements by avoiding DNA strand breaks [19]. Whether both pathways also act on ICLs induced by other cellular aldehydes is not known but one of these, acrolein, has been linked to the FA pathway [20–24]. Combined deficiency in the FA pathway and aldehyde dehydrogenase 9A1 (ALDH9A1) leads to synthetic lethality in cells and solid tumours in mice, likely due to increased endogenous acrolein levels [25]. Exposure to acrolein is enhanced by smoking [26, 27], which leads to increased levels of acrolein monoadducts, ICL precursors implicated in alcohol- and smoking-related cancers. However, whether acrolein-ICLs require the FA pathway, or the excision-independent pathway, or both, for their repair has not yet been demonstrated.

TLS past an unhooked adduct is an essential step for both the FA and excision-independent pathways. TLS typically involves two steps: (i) insertion of a nucleotide opposite the lesion followed by (ii) DNA extension past the lesion. These steps involve specialized polymerases that can accommodate modified or damaged bases in their active sites [28–31]. In eukaryotes, these are the Y-family polymerases Rev1, Polκ, Polη, and Polι and the B-family polymerase Polζ, consisting of the catalytic subunit Rev3 and the co-subunits Rev7, Pold2, and Pold3 [32–35]. Recruitment of these specialized polymerases often occurs via PCNA, which gets ubiquitylated in response to DNA damage [36–42] and interacts with TLS polymerases through their PCNA interacting domains (PIPs) and ubiquitin-binding zinc fingers (UBZs) or motifs (UBMs) [33, 34, 42, 43]. Rev1 acts as a scaffold for Y-family polymerases and Polζ and can alternatively promote their recruitment [28, 30, 31]. The role of these TLS polymerases in ICL repair, especially during the insertion step, is still unknown.

Studying TLS during interstrand crosslink repair has proven to be challenging, partly because crosslinking agents induce various damage types requiring different repair pathways and because the exact nature of the adduct after ICL unhooking is not always known. Previous studies in *Xenopus* egg extract showed that Rev1–Polζ is important for extension past the unhooked adduct in the repair of cisplatin ICLs but not for the less distorting nitrogen mustard-like ICLs [14, 17]. While the Rev1–Polζ complex also plays a role in acetaldehyde ICL repair, loss of this complex affects TLS at the stage of insertion [19]. In *in vitro* primer extension assays, another TLS polymerase, Polκ, can bypass substrates mimicking FA-mediated unhooked Pt-ICLs, ACR-ICLs, and nitrogen mustard-ICLs [28]. Polκ and its bacterial orthologue PolIV show specificity for the bypass of minor groove lesions, including the N2-guanine aldehyde adducts [44–47]. However, the role of Polκ in aldehyde ICL repair has not been explored in a physiological setting.

In this study, we first show that acrolein ICLs, like acetaldehyde ICLs, are repaired via both the FA pathway and the recently identified excision-independent pathway, thereby establishing a common repair strategy for aldehyde-induced ICLs. We next focus on the FA pathway-mediated repair route and identify Polκ as the primary TLS polymerase in aldehyde ICL repair, promoting the insertion step in TLS. Our data indicate Polκ is recruited to aldehyde ICLs via PCNA. While the bypass of aldehyde-ICL adducts by Polκ does not depend on Rev1, we show that Polκ has a Rev1-dependent role in the bypass of cisplatin adducts during ICL repair. Together our data suggest that the mechanisms of ICL repair differ substantially between model chemotherapeutic lesions such as cisplatin and lesions caused by endogenous reactive aldehydes *in vivo*.

Materials and methods

Synthesis of site-specific native acrolein ICL and acrolein monoadduct duplexes

Oligodeoxyribonucleotide (ODN) duplexes containing γ-OH-PdG (mono-ACR) and native acrolein ICL (ACR_{NAT}-ICL) were generated using a similar method as in [19]. Briefly, a custom GA-rich ODN 'ACR_{NAT}-GA-2FdI' (5′-[phos]-GCA CGA AAG AAG AGC 2FdI-GA AG, Eurogentec, Oligo 1, Table 1) was synthesized, including a 5′-Dimethoxytrityl-2-fluoro-O^6-(p-nitrophenylethyl)-2′-deoxyinosine,3′-[(2-cyanoethyl)-(*N*,*N*-diisopropyl)]-phosphoramidite. The ODN (ca. 0.25 μmol ODN on solid support) was incubated with 7 mg 4-amino-1,2-butanediol (FluoroChem) in 220 μl DMSO and 110 μl TEA with agitation at room temperature (RT) overnight. The support was washed three times with 200 μl DMSO and three times with 400 μl CH_3CN, followed by removal of the O^6-p-nitrophenylethyl group with 300 μl of 1 M DBU in CH_3CN at RT for 1 h. The support was washed three times with 250 μl CH_3CN and treated with 500 μl aq. Twenty-eight percent NH_4OH at 55°C for 6 h to remove the remaining protecting groups and elute the N^2-(3,4-dihydroxybutyl)-guanine-modified ODN from the support. The ODN was dried using a SpeedVac, resuspended in water, applied to a MonoQ 5/50 GL column in buffer A (10 mM

Table 1. All oligos used in this study

Primer #	Used for	Sequence	Notes
1	Native Acrolein ICL duplex formation	5′-[phos]-GCACGAAAGAAG AGC 2FdI-GA AG	ACR_{NAT}-GA-2FdI
2	Native Acrolein ICL duplex formation	5′-[phos]-CCCTCTTCCGCT CTTCTTTC	ACR_{NAT}-CT
3	Native Acrolein ICL position confirmation	5′-[phos]-CCCTCTTCC-dI-CT CTTCTTTC	ACR_{NAT}-CT-dI
4	Reduced Acrolein ICL duplex formation	5′-[phos]-GCACGAAAGAAGCAC-2FdI-TGAG	ACR_{RED}-GA-2FdI
5	Reduced Acrolein ICL duplex formation	5′-[phos]-CCCTCTCAC-2FdI-TGCTTCTTTC	ACR_{RED}-CT-2FdI
6	Control sequence for Reduced Acrolein ICL duplex formation	5′-[phos]-GCACGAAAG AAGCACGTGAG	
7	Control sequence for Reduced Acrolein ICL duplex formation	5′[phos]-CCCTCTCACGTGCTTCTTTC	
8	Sequencing ladder production	5′CATGTTTTACTAGCCAGATTTTTC CTCCTCTCCTG	Primer S (USB)
9	Primer extension on late repair products Forward	5′CTCGAGCGGAAGTGCAGAAC	
10	Primer extension on late repair products Reverse	5′AATACGCAAACCGCCTCTCC	
11	MutSeq Step 1 Reverse	5′GTTCAGACGTGTGCTCTTCCGATCT NNNNNNNNNNNNNNNNBBBBBBBB GGGGCGGGACTATGGTTGCTGACT	GTTCAGACGTGTGCTCTTCCGATCT = Nesting Sequence for Step 2 NNNNNNNNNNNNNNNN = UMI BBBBBBBB = Barcode *See Barcode list below table
12	MutSeq Step 2 Forward	5′CTCCTGACTACTCCCAGTCATAGC TGTCCC	
13	MutSeq Step 2 Reverse	5′GTTCAGACGTGTGCTCTTCCGATC T	
14	Amplification GST HRV-3C from pGex6p2 for Gibson Assembly Forward	5′TCGACGAGCTCACTTGTCGCCATG TCCCCTATACTAGGTTATTGGAAAAT TAAGG	Compatible with NotI digested pACEBac1
15	Amplification GST HRV-3C from pGex6p2 for Gibson Assembly Reverse	5′CAGGCTCTAGATTCGAAAGCGGCC GCGGGCCCCTGGAACAGAAC	Compatible with NotI digested pACEBac1
16	*xl*Polκ Wt Gibson Assembly fragment Forward	5′GGCTCTAGATTCGAAAGCTTATCA CTTAAAAAATCGATCTATAGTATTTT TCGAAGAATTAGGTTTTC	Arms were incorporated into 1992 bp gBlock containing codon optimized xlWT Polκ for Gibson Assembly. Compatible with NotI digested pACEBac1-GST HRV 3C
17	*xl*Polκ Wt Gibson Assembly fragment Reverse	5′GTTCCAGGGGCCCGCAAT GGACAATAAGCAGGAGGCC	Arms were incorporated into 1992 bp gBlock containing codon optimized xlWT Polκ for Gibson Assembly. Compatible with NotI digested pACEBac1-GST HRV 3C
18	*xl*Polκ RIR mt Gibson Assembly fragment production Forward	5′CTCGGCAGTGACAAGGAGGTGCAG TGC	Arms were incorporated into 400 bp gBlock containing RIR mutation for Gibson Assembly. Compatible with pACEBac1-GST HRV 3C-PolκWT
19	*xl*Polκ RIR mt Gibson Assembly fragment production Reverse	5′GGCTTTCCGCTATGGAGGAACGAG GTT	Arms were incorporated into 400 bp gBlock containing RIR mutation for Gibson Assembly. Compatible with pACEBac1-GST HRV 3C-PolκWT
20	Site directed mutagenesis Polκ CD mutant Forward	5′CAACTTTCTCCCTATGTCGCTG GcTGc AGCTTACCTCGATTTCACTGACC	Polκ D199A, E200A; catalytic dead mutant. Compatible with pACEBac1-GST HRV 3C-PolκWT**
21	Site directed mutagenesis Polκ CD mutant Reverse	5′GGTCAGTGAAATCGAGGTAAGC TgCAg CCAGCGACATAGGGAGAAAGTTG	Polκ D199A, E200A; catalytic dead mutant. Compatible with pACEBac1-GST HRV 3C-PolκWT**
22	Site directed mutagenesis Polκ PIP1 mutant Forward	5′GCACCACCAGAAGTCTATAACCTC GgcCCg CCATAGCGGAAAGCCAGGC	Polκ F530A, L531P; PIP1 mutant Compatible with pACEBac1-GST HRV 3C-PolκWT**
23	Site directed mutagenesis Polκ PIP1 mutant Reverse	5′GCCTGGCTTTCCGCTATGGcGGgc CGAGGTTATAGACTTCTGGTGGTGC	Polκ F530A, L531P; PIP1 mutant Compatible with pACEBac1-GST HRV 3C-PolκWT**
24	Site directed mutagenesis Polκ PIP2 mutant Forward	5′GTAAGAAATCAAAACCTAATTCTT CGAAAAATACTATAGATCGAgcTgc TAAGTGATAAGCTTTCGAACTAGAGC CTG	Polκ F860A, F861A; PIP2 mutant Compatible with pACEBac1-GST HRV 3C-PolκWT**
25	Site directed mutagenesis Polκ PIP2 mutant Reverse	5′CAGGCTCTAGATTCGAAAGCTTAT CACTTAgcAgc TCGATCTATAGTATTTTTCGAAGAAT TAGGTTTGATTTCTTAC	Polκ F860A, F861A; PIP2 mutant Compatible with pACEBac1-GST HRV 3C-PolκWT**
26	Site directed mutagenesis Polκ UBZ1 mutant Forward	5′GGATGGGATATCGCTACCTTTAAT AAACATATCGc CAAGTGCCTCTCGGGTTCTC	Polκ D634A; UBZ1 mutant Compatible with pACEBac1-GST HRV 3C-PolκWT**
27	Site directed mutagenesis Polκ UBZ1 mutant Reverse	5′GAGAACCCGAGAGGCACTTGg CGATATGTTTATTAAAGGTAGCGATA TCCCATCC	Polκ D634A; UBZ1 mutant Compatible with pACEBac1-GST HRV 3C-PolκWT**

Table 1. Continued

Primer #	Used for	Sequence	Notes
28	Site directed mutagenesis Polκ UBZ2 mutant Forward	5′GACGGCCTTTAATCGCCATGTTGc TGTTTGTTTAAATAAGGGTATTATTC AAAAGCTCACAGAG	Polκ D789A; UBZ2 mutant Compatible with pACEBac1-GST HRV 3C-PolκWT**
29	Site directed mutagenesis Polκ UBZ2 mutant Reverse	5′CTCTGTGAGCTTTTGAATAATACC CTTATTTAAACAAACAg CAACATGGCGATTAAAGGCCGTC	Polκ D789A; UBZ2 mutant Compatible with pACEBac1-GST HRV 3C-PolκWT**
30	*In vitro* primer extension by *xl*Polκ	5′CGGCCGCTCTACAACTAGTGGATC CATGCACGCTGTCTAGAGGAAGCC GGTAATAGCTACGTAGCGTCTAGCTA GGAGCTGTCTTCATGAATTCGATATC	
31	*In vitro* primer extension by *xl*Polκ	5′GATATCGAATTCATGAAGACAGC TCCTAGCTAGAC	conjugated to an Alexa Fluor 647 on the 5′ end

All primers and gBlocks were obtained from IDT unless otherwise specified in the 'Materials and methods' section.
* Barcodes used for MutSeq: ACGTAGCT, CGTCGGCT, GCGTTTCG, GGTCTGAC, GTTTCACT, TACGAATC, CCTTTACA, CTAGATTC, ACTAACTG, and ATCCTATT.
**Mutant bases for mutagenesis are indicated by lower cases. All generated plasmids were verified by sequencing.

Tris–HCl, pH 7.5, 100 mM NaCl), and eluted in a gradient of 3% buffer B (10 mM Tris–HCl, pH 7.5, 800 mM NaCl) per CV at 4°C. The N^2-(3,4-dihydroxybutyl)-guanine-modified ODN eluted at a conductivity of 46.1 mS/cm. Peak fractions were pooled and reinjected to increase purity followed by desalting using a NAP-5 column (Cytiva). The modified ODN was reacted with 50 mM $NaIO_4$ for 1 h at RT and the reaction was quenched by desalting over a NAP-5 column in MQ water. The resulting γ-hydroxy-1,N^2-propanoguanine-modified (γ-OH-PdG) ODN was mixed at a 1:1 molar ratio with the complementary CT-rich ODN 'ACR_{NAT}-CT' (5′-[phos]-CCC TCT TCC GCT CTT CTT TC, Oligo 2, Table 1) in PBS and annealed (85°C for 5 min, ramped to 25°C at −0.1°C s^{-1}) and flash frozen immediately to prevent crosslink formation. The presence of mono-ACR adduct was confirmed by primer extension assay (Supplementary Fig. S1G).

For native acrolein ICL (ACR_{NAT}-ICL) formation, the annealed ODNs were incubated at 37°C for 7–14 days to allow cross-link formation. The reaction progression was analysed by denaturing polyacrylamide gel electrophoresis (PAGE) stained with Sybr Gold (Thermo Scientific) (Supplementary Fig. S1E). Final γ-OH-PdG-dG crosslink yields were ∼50%. Crosslinked duplexes were purified by denaturing PAGE and/or High-Performance Liquid Chromatography (HPLC) via an AdvanceBio Oligonucleotide, 4.6 × 150 mm, 2.7 μm column (Agilent) in 15 mM TEA/400 mM HFIP (pH 7.0), at 0.5 ml min^{-1} at 60°C, over 30 min, effecting a 25%–32.5% MeOH gradient. Crosslinked ODN duplexes eluted at ∼30% MeOH and were confirmed by denaturing PAGE analysis. Fractions containing crosslinked DNA were evaporated to dryness and reconstituted in 1× PBS. The identity of the crosslinked ODN duplexes was confirmed by MALDI MS (M_{exp} 12353 Da, M_{obs} 12357 Da, equivalent to an accuracy of ca. 300 ppm).

The γ-OH-PdG ODN was also annealed and incubated with a 2′-deoxyinosine-containing ODN 'ACR_{NAT}-CT-dI' (5′-[phos]-CCC TCT TCC -dI-CT CTT CTT TC, oligo 3, Table 1) to confirm crosslinking to the correct nucleotide (Supplementary Fig. S1C).

Synthesis of site-specific reduced acrolein ICL duplexes

For direct preparation of reduced acrolein interstrand crosslinks (ACR_{RED}-ICL), two ODNs containing a PmlI restriction site were synthesized by LGC Biosearch or Eurogentec.

A GA-rich ODN 'ACR_{RED}-GA-2FdI' (5′-[phos]-GCACGAAAGAAGCAC-2FdI-TGAG, Oligo 4, Table 1) was prepared as described earlier, or in a control reaction omitting 4-amino-1,2-butanediol. In either case, the 2FdI-containing deprotected oligonucleotide was purified by HPLC using an AdvanceBio Oligonucleotide, 4.6 × 150 mm, 2.7 μm column (Agilent), using buffers and conditions described earlier, effecting a 20%–27.5% MeOH gradient over 30 ml. Fractions containing deprotected 2FdI were collected at ∼24% MeOH. After drying, oligo was resuspended in pure water. Final mass was determined by MALDI (M_{exp} 6292 Da, M_{obs} 6292 Da). A complementary CT-rich ODN 'ACR_{RED}-CT-2FdI' (5′-[phos]-CCCTCTCAC-2FdI-TGCTTCTTTC, Oligo 5, Table 1) was synthesized using base-labile phosphoramidites (phenoxyacetyl (pac) for dA and dG and acetyl for dC), incorporating an O^6-(2-trimethylsilyl)-2-fluoro-2′-deoxyinosine CED phosphoramidite. ODN ACR_{RED}-CT-2FdI (0.5 μmol on support) was reacted with 1 ml of 50% 1,3-Diaminopropane in DMSO and incubated at RT for 24 h. Beads were reconstituted in pure water, to which an equal volume of 10% AcOH was added (to 5% final concentration), and incubated for 45 min at RT, after which the reaction was neutralized on ice, with an equal volume of 1M K_2HPO_4. Eluted oligo was desalted using a Nap-10 column (Cytiva) and final mass was confirmed by MALDI (M_{exp} 6083 Da, M_{obs} 6082 Da).

Equimolar amounts (1 nmol each) of the two oligos were annealed in 1× PBS and allowed to react up to 4 d at RT. The resulting crosslinked duplex was purified over an AdvanceBio Oligonucleotide column under conditions described for PK2FPi2_PmlI_top. ACR_{RED}-ICL was readily separated from non-reacted species at 25% MeOH. Crosslink formation was confirmed by denaturing PAGE and final mass was confirmed by MALDI MS (M_{exp} 12355 Da, M_{obs} 12358 Da, equivalent to an accuracy of ca. 200 ppm) (Supplementary Fig. S1B).

Synthesis of other site-specific ICL-containing duplexes

Oligo duplexes containing a native acetaldehyde ICL (AA_{NAT}-ICL) or a Me-γ-OH-PdG (mono-AA) were prepared as described in [19]. The reduced acetaldehyde ICL (AA_{RED}-ICL)-containing duplex was prepared as described in [48], and cisplatin ICL (Pt-ICL) duplex was prepared as described in [14].

Crosslink stability assay

Aliquots (3 μl) of crosslinking reactions prior to purification were incubated with 3 μl of a 6.25% formic acid solution for 10 min at 37°C. Reactions were quenched with 10 μl of 1 M Tris–HCl (pH 8.0), and 15 μl of Gel Loading Buffer II (Invitrogen™) was added. Products were separated on 18% denaturing PAGE gel and stained with SybrGold.

Preparation of plasmids

ICL-containing plasmids were prepared as described previously [19, 48–51]. Briefly, duplexes containing ICLs derived from acetaldehyde, acrolein, cisplatin, or psoralen were ligated into a pSVRLuc vector linearized with Bbs1. After ligation, the plasmid was purified using a caesium chloride gradient. To make pMono-AA or pMono-ACR, ligation of a duplex containing a PdG into a backbone linearized by Bbs1 was followed by caesium gradient purification, as described earlier. pCtrl-ACR was prepared by annealing the primers 6 and 7 of Table 1, followed by ligation of the duplex into BbsI-digested pSVRluc.

Preparation of *Xenopus* egg extracts

Xenopus laevis female frogs (aged >2 years) were purchased from Nasco, which provided eggs. Preparation of *Xenopus* egg extracts and DNA replication were performed as previously described [52, 53]. All animal procedures and experiments were performed in accordance with national animal welfare laws and were reviewed by the Animal Ethics Committee of the Royal Netherlands Academy of Arts and Sciences (KNAW). All animal experiments were conducted under a project licence granted by the Central Committee Animal Experimentation (CCD) of the Dutch government and approved by the Hubrecht Institute Animal Welfare Body (IvD), with project licence number AVD80100202216633.

Replication of plasmids in *Xenopus* egg extract

For DNA replication, plasmids were incubated in a high-speed supernatant extract (HSS) at a final concentration of 7.5 ng/μl for 20–30 min at RT to license the DNA. Two volumes of nucleoplasmic extract (NPE) were added to start DNA replication. For nascent strand labelling, HSS was supplemented with 32P-α-dCTPs. When indicated, an unrelated non-damaged control plasmid (pQuant) of 3.8 kb was added at concentrations up to 0.8 ng/μl, to be used as internal control for quantifications [19]. CMG unloading was blocked by the addition of p97 inhibitor (NMS-873, Sigma) to NPE at a final concentration of up to 200 μM 20 min before the start of replication [19]. To analyse undigested DNA replication products, replication reactions were stopped by adding five volumes of replication stop solution I [Stop I: 80 mM Tris (pH 8), 5% sodium dodecyl sulphate (SDS), 0.13% phosphoric acid, 10% Ficoll, 8 mM ethylenediamine tetraacetic acid (EDTA), 0.1% bromophenol blue]. The samples were treated with proteinase K (1.5 μg/μl) for 30 min at 37°C and resolved by 0.8% native agarose gel electrophoresis. The gel was dried and visualized by autoradiography. For isolation of replication intermediates, aliquots of the reaction were stopped with 10 volumes of replication stop solution II (Stop II: 50 mM Tris (pH 7.5), 0.5% SDS, 10 mM EDTA pH 8). Samples were then treated with Proteinase K (0.5 μg/μl) for 1 h at 37°C or overnight at RT. DNA was phenol/chloroform extracted, ethanol precipitated with glycogen (0.3 μg/μl), and resuspended in 10 mM Tris, (pH 7.5), in a volume equal to the reaction sample taken.

Immunodepletion

Polκ and Rev1 depletion were carried out as follows: Dynabeads Protein A (ThermoFisher) were saturated with purified antibody overnight at 4°C or for 30 min at RT. Antibody-coupled beads were incubated in NPE and HSS in a 3:1 ratio for 30 min at 4°C for one round. For mock depletions purified IgGs were used. In the experiments where double depletions are compared to single depletions, the bead-to-extract volume was kept identical via supplementation of mock beads to the single depletions. To rescue depletions with wild-type (WT) or mt Polκ, near-endogenous levels of recombinant Polκ were added to the depleted extract before the start of replication. The final protein levels in the extract were determined by western blot.

Antibodies

For depletion and detection of *Xenopus* Polκ antibodies, they were generated via Vivitide, who produced C- and N-terminal peptide antigens, injected them in rabbits and purified their antisera. C-term Polκ: Ac-C KSKPNSSKNTIDRFFK-OH, N-term Polκ: H2N-MDNKQEAEIAPSNEAFQC-amide. Both antibodies, and not their pre-immune sera, were capable of detection and depletion of Polκ. For all depletions and western blot analyses, the C-terminal antibody was used. Only in the cases where the recombinant PIP mutant of Polκ had to be detected did we use the N-terminal antibody, as the PIP2 is at the C-terminus. For depletion and detection of Rev1 and FANCD2, antibodies were generated via Biogenes: Rev1 [17] and FANCD2 [14, 15]. Antigens were expressed in bacteria and purified as previously reported. gBlocks (IDT) were ordered of *Escherichia coli* codon-optimized antigens against *Xenopus*, a middle fragment of Rev1 (aa: 120–420), and an N-terminal fragment of FANCD2 (aa: 1–117). The use of antibodies against xlREV7 [14, 15, 17, 19] and PCNA [17, 54] and Histone H3 (abcam) was previously described. The antibody for Ubiquityl-PCNA Lys164 is available commercially at Cell Signaling Technology (D5C7P) Rabbit mAb #13439.

Repair assay

Repair as measured by restriction recognition site regeneration was analysed by digesting 1 μl of extracted DNA with HincII (New England Biolabs), or HincII and SapI (New England Biolabs) for Pt-ICLs, or HincII and PmlI (New England Biolabs) for ACR_{RED}-ICLs for 3 h at 37°C. The resulting products were separated on a 0.8% native agarose gel. The gel was dried and visualized by autoradiography. Repair efficiency was calculated as previously described [15].

APEI glycosylase assay

Strand breaks or abasic site formation was assessed as previously described [19]. Briefly, plasmids were replicated in the presence of pQuant. After extraction of the DNA repair intermediates, samples were digested with HincII or with HincII and APE1 (New England Biolabs). The digested products were separated on a 0.8% native agarose gel, and the gel was dried and visualized by autoradiography. Quantification was done

using Image Quant (GE Healthcare). The arm fragments were first normalized against pQuant, and the highest value was set to 1.

Sequencing gel

Nascent strand analysis was performed as previously described [14]. In brief, extracted DNA repair products were digested with AflIII (New England Biolabs) for 3 h at 37°C. After adding one volume of denaturing PAGE Gel Loading Buffer II (Invitrogen™), the samples were separated on a 7% polyacrylamide sequencing gel; the gel was dried and visualized by autoradiography. The sequencing gel ladder was produced using the Thermo Sequenase Cycle Sequencing Kit containing ddNTPs (USB), a pCtrl plasmid and primer 8 (Table 1).

Lesion bypass assay

Extracted DNA repair products were digested with HincII and separated on an alkaline 0.8% agarose gel. The gel was dried and visualized by autoradiography. Relative arm and bypass products were quantified by normalizing their intensities with the corresponding pCDF radioactive signal. The highest measured intensity of the mock conditions was set to 1.

NotI assay

NotI assays were performed as described in [19]. Briefly, plasmids were replicated in *Xenopus* egg extract in the absence of 32P-α-dCTPs, and intermediates were purified as described earlier. Replication reactions were supplemented with a pQuant plasmid that produces a 28-nt fragment upon NotI digestion as an internal control. Extracted DNA was digested with NotI-HF for 2 h at 37°C and 3′ labelled by filling in the 5′-overhangs with Sequenase DNA Polymerase (USB) in the presence of 32P-α-dCTPs and non-labelled dGTP. One volume of denaturing PAGE Gel Loading Buffer II (Invitrogen™) was added, samples were denatured by incubation at 98°C for 3 min, kept on ice, and the DNA fragments were separated by 20% urea PAGE. Products were visualized by autoradiography and quantified using ImageQuant software (GE Healthcare). To quantify repair percentages, first, the intensity of pQuant 28 nt fragment was used to normalize the intensity of the 44 nt products. Then, the normalized linear 44-nt products were expressed as a percentage of the total of 88- and 44-nt fragments at time point zero, which represents the percentage of the input DNA that is accumulating over time in the 44-nt band. Finally, the percentage of non-crosslinked background was subtracted to yield the percentage of molecules that have undergone TLS or HR during repair. Of note, 2 or 3 bands can be seen at the height of the 44-nt fragment in some gels as described previously [19].

Primer extension on late repair products

Primer extensions were performed as described in [19]. Briefly, plasmids were replicated in *Xenopus* egg extract in the absence of 32P-α-dCTPs, and late replication and repair products were purified as described earlier. Samples were digested with AflIII and BamHI, and the DNA fragments were used as a template for primer extension with either a forward primer, primer 9, or reverse primer, primer 10 (Table 1), that was radioactively labelled with PNK and 32P-γ-ATP at the 5′ end and was subsequently annealed to DNA in a thermocycler. The primers were then extended using the Phusion High-Fidelity DNA Polymerase (NEB) for one round. The resulting DNA fragments were first concentrated by ethanol precipitation (as described earlier) and then separated on a 20% denaturing PAGE gel and visualized by autoradiography.

Mutation sequencing sample preparation

To generate MutSeq libraries, phenol-chloroform-extracted DNA from late replication reactions was treated with 2 μg RNaseA at 37°C for 1 h. Ten nanograms of RNase-treated DNA was then amplified during a two-step nested polymerase chain reaction (PCR). Step 1 involves a single PCR cycle with an equimolar ratio of input DNA and a single barcoded and Unique Molecular Identifier (UMI)-containing primer 11 (Table 1), adding a sample-specific barcode (8 nt), a 16 nt UMI for quantification, and nesting sequences for step 2. Step 2 primers, primers 12 and 13 (Table 1), added indexes and Illumina p5/p7 sequences and amplified the barcode-tagged samples. Samples are analysed for the specific amplification product on an agarose gel, extracted (Promega Wizard kit), and pooled together. Final pooled libraries were quantified by Qubit (Thermo Fisher) and sequenced on the MiSeq with paired-end reads (Eurofins). All kits & reagents were used following manufacturer's protocols unless otherwise stated. PCR was carried out with Herculase II Fusion DNA polymerase (Agilent).

Mutation sequencing data analysis

Paired raw 150 bp short-read data received from Eurofins (commercial Illumina sequencing provider) were demultiplexed based on associated barcodes using Je-Demultiplex [55], with UMIs subsequently extracted from reads using UMItools [56]. Trim-Galore was then used to trim Illumina adapter sequences prior to alignment to the reference genome using bwamem2 [57], followed by read deduplication using UMItools. Processed reads were merged using FLASH prior to generation and analysis of mutation profiles using SIQ [58]. Visualization was performed in R.

Plasmid pulldown

Plasmid DNA was replicated in egg extracts at 5 ng/μl (final concentration). At the indicated time points, 8–10 μl of the reaction was taken for plasmid pulldown using biotinylated LacI-coated beads [17]. After 30 min incubation at 4°C, samples were washed twice in 10 mM HEPES (pH 7.7), 50 mM KCl, 2.5 mM $MgCl_2$, 0.03% Tween 20, and once in 10 mM HEPES, pH 7.7, 50 mM KCl, 2.5 mM $MgCl_2$ [59]. Sample preparation for mass spectrometry was different for the two experiments and therefore separately described below.

Mass spectrometry of plasmid-bound proteins from undepleted extract

The DNA-bound factors isolated by plasmid pulldown were separated on a 12% Bis-Tris SDS–PAGE gel (Bio-Rad). The gel was run for ∼2–3 cm, stained with colloidal Coomassie dye G-250 (Gel Code Blue Stain Reagent, Thermo Scientific), and each lane was cut into three pieces. Gel pieces were reduced, alkylated, and trypsinized overnight at 37°C. Peptide extraction was done with 100% acetonitrile (ACN), and samples were dried in a vacuum concentrator. Samples were resuspended in 10% (v/v) formic acid for UHPLC-MS/MS. Data acquisition was done using a UHPLC 1290 system coupled

to an Orbitrap Q Exactive Biopharma HF mass spectrometer (Thermo Scientific). Samples were first trapped (Dr Maisch Reprosil C18, 3 μm, 2 cm × 100 μm) for 5 min at 5 μl min^{-1} in solvent A (0.1 M acetic acid in water). Samples were then separated on an analytical column (Agilent Poroshell EC-C18, 278 μm, 40 cm × 75 μm), at a column flow of 300 nl min^{-1} with a gradient as follows: 13%–44% solvent B (0.1 M formic acid in 80% acetonitrile) in 95 min, 44%–100% in 3 min, 100% solvent B for 1 min, and 100%–0% in 1 min. The acquisition of full scan MS spectra was performed at m/z 375–1600, at a resolution of 60 000 at m/z 400 after accumulation to a target value of 3e6. Up to ten of the most intense precursor ions were selected for HCD fragmentation, which was done at a normalized collision energy of 27% after the accumulation of the target value of 1e4. MS/MS acquisition was at 30 000 resolution. Raw data files were analysed using the MaxQuant software (version 1.5.0.17) with label-free quantification [60]. A false discovery rate of 0.01 and minimum peptide length of 7 amino acids were used. A non-redundant *Xenopus* database [61] was used as a search engine for the data. Cysteine carbamidomethylation was selected as a fixed modification, while protein N-terminal acetylation and methionine oxidation were selected as variable modifications. For the Andromeda search, trypsin was chosen as enzyme allowing for N-terminal cleavage to proline. A maximum of two missed cleavages was allowed. The mass deviation for fragment ions was 0.5 Dalton, and the initial mass deviation of precursor ions was up to 7 ppm. All bioinformatics analysis was carried out with the Perseus software version 1.6.10.0. For each comparison, the processed data was filtered to contain at least two valid values in at least one of the replicate groups (three repeats per condition).

Mass spectrometry of plasmid-bound proteins from depleted extract

The DNA-bound factors isolated by plasmid pulldown samples were washed in 50 μl of 10 mM HEPES (pH 7.7), 50 mM KCl, 2.5 mM MgCl2, and transferred to a new tube to remove residual detergent. Beads were dried out and resuspended in 50 μl denaturation buffer (8 M urea, 100 mM Tris, pH 8.0). Cysteines were reduced (1 mM TCEP, 15 min at RT) and alkylated (5 mM iodoacetamide, 45 min at RT). Proteins were digested and eluted from beads with 1.5 μg LysC (Promega) for 2.5 h at RT. Eluted samples were transferred to a new tube and diluted 1:4 with ABC (50 mM ammonium bicarbonate). 2.5 μg trypsin (Merck Sigma) was added and incubated for 16 h at 30°C. NaCl was added to 400 mM final concentration, and peptides were acidified and purified by stage tipping on C18 material (Pierce ThermoFisher). MS experiments were carried out in quadruplicate. LC-MS/MS analysis was carried out using nanoLC-MS/MS on an Orbitrap Astral mass spectrometer (Thermo Scientific) coupled to a Vanquish Neo nanoLC system (Thermo Scientific). The Vanquish Neo was run in trap-and-elute mode, with peptides first loaded onto a Pepmap 100 C18 5 μm trap column (300 μm × 5 mm, Thermo Scientific), followed by separation on an analytical column (AUR3-25075C18-TS, 1.7 μm/75 μm × 25 cm, IonOpticks AU) installed in an Easyspray ion source (Thermo Scientific) and operated with a spray voltage of 1350 V. The column was maintained at 50°C, and the initial flow rate was set to 0.5 μl/min to reduce delay. Solvents consisted of 0.1% formic acid in water (solvent A) and 0.1% formic acid in 80% acetonitrile (solvent B). Peptides were eluted at a flow rate of 0.4 μl/min using a 36-min gradient: an initial non-linear rise from 8% to 45% solvent B, followed by a 0.4-min ramp to 99% solvent B, and a 5.4-min wash at 0.5 μl/min. Column equilibration was then performed using a 'fast equilibration' script in combined control mode with a maximum pressure of 1450 bar. The Orbitrap Astral mass spectrometer operated in data-independent acquisition (DIA) mode. Full MS scans were acquired in the Orbitrap analyser at a resolution of 240 000 (m/z 200) over the range of 380–980 m/z. The default charge state was set to 2^+, with a normalized AGC target of 500% (equivalent to 5×10^6 charges) and a maximum injection time of 5 ms. For DIA MS2 scans, a normalized HCD collision energy of 25% was applied across the precursor range of 380–980 m/z, using non-overlapping 2 m/z isolation windows with window placement optimization enabled. MS2 spectra were collected in the Astral analyser over a range of 100–1000 m/z, with the normalized AGC target set to 500% (equivalent to 5×10^4 charges) and a maximum injection time of 3 ms. All raw mass spectrometry spectra were processed using DIA-NN software (version 1.8.0 or later) [62] according to developers' guidelines.

Cloning *Xenopus* Polκ

Wildtype Polκ. First, GST and an H3V-3C site were cloned from pGex6p2 in pACEBac1 via Gibson assembly using NotI-digested pACEBac1 and the forward and reverse primers 14 and 15, producing pACEBac1-GST-HRV-3C with a regenerated NotI site downstream of the HRV-3C site. pACEBac1-GST-HRV-3C-Polκ wt was then created via Gibson assembly using NotI-digested pACEBac1-GST-HRV-3C and a gBlock (IDT) containing *Xenopus laevis* WT codon optimized for *Spodoptera frugiperda* and the required Gibson arm (primers 16 and 17) already attached. The resulting plasmid has been verified by sequencing. Polκ F562A, F563A Rev1 interaction mutant was generated via Gibson assembly by linearizing vector pACEBac1-GST HRV-3C-$Polκ^{wt}$ using primers 18 and 19, and ligating a gBlock (IDT) containing the Polκ RIR mutant sequence with the arms required for Gibson assembly already incorporated. Other mutants of Polκ were generated in pACEBac1-GST HRV-3C-Polκwt via site-directed mutagenesis using primers 20–29. Mutant bases are underlined, and all mutations have been confirmed by sequencing.

Polκ expression and purification

Baculoviruses were produced using the MultiBac system following the manufacturer's protocol (Geneva Biotech) in competent DH10Bac cells. Approximately 3.6×10^9 virus-infected *Spodoptera frugiperda* (sf9) insect cells grown in Sf-900™ III SFM (Gibco) were harvested 65 h post-infection. Cells were resuspended in 70 ml of buffer containing 10 mM Tris–HCl (pH 7.5), 10 mM PBS (pH 7.6), 0.5% Triton X-100, 300 mM NaCl, 1 mM EDTA, and 1 mM DTT supplemented with 1 mM PMSF and EDTA-free protease inhibitor (Roche) and lysed by sonication. After sonication, the cell suspension was treated with 20 units of DNase-Turbo (Invitrogen) for 20 min at 4°C. The suspension was cleared from insoluble material via centrifugation, and the supernatant was added to 2.4 ml Glutathione Sepharose® 4B beads (Cytiva) and incubated for 2 h at 4°C. The resin was washed with 10 column volumes (CV) of 10 mM Tris–HCl (pH 7.5), 10 mM PBS (pH 7.6), 0.5% Triton X-100, 300 mM NaCl, 1

mM EDTA, and 1 mM DTT with protease inhibitors. The washed beads were reconstituted in 25 ml of buffer containing 10 mM Tris–HCl (pH 7.5), 10 mM PBS (pH 7.6), 0.5% Triton X-100, 300 mM NaCl, 1 mM EDTA, and 1 mM DTT, loaded onto a 20 ml Econopac disposable column (Bio-Rad), and washed with 2.5× CV buffer containing 10 mM Tris–HCl (pH 7.5), 10 mM PBS (pH 7.6), 10% glycerol, 300 mM NaCl, 1 mM EDTA, and 1 mM DTT with protease inhibitors followed by 1.25× CV without protease inhibitors. Polκ was eluted on beads by incubation with 80 units of PreScission protease (Cytiva) for 2 h at 4°C. Fractions were pooled based on SDS–PAGE analysis and loaded onto a HiTrap Heparin column 1 ml (Cytiva) equilibrated in 10 mM Tris–HCl (pH 7.5), 10 mM PBS (pH 7.6), 10% glycerol, 300 mM NaCl, 1 mM EDTA, and 1 mM DTT and eluted in a linear gradient of 20 CV in 10 mM Tris–HCl (pH 7.5), 10 mM PBS (pH 7.6), 1 M NaCl, 10% glycerol, 300 mM NaCl, 1 mM EDTA, and 1 mM DTT. Polκ eluted at a conductivity of 39.50 mS/cm. Fractions were monitored by SDS–PAGE, concentrated, and injected onto a Superdex 200 Increase 10–300 GL size exclusion column (Cytiva), equilibrated in 50 mM Tris–HCl (pH 7.5), 300 mM NaCl, 1 mM EDTA, 1 mM DTT, and 5% glycerol. Eluted Polκ was concentrated to ∼1–1.2 mg/ml, flash frozen in liquid nitrogen, and stored at −80°C. Mutants of Polκ were purified as described for the WT and behaved the same way during purification. All proteins were validated by SDS–PAGE analysis and Coomassie or InstantBlue® Coomassie Protein Stain (Abcam).

In vitro primer extension

To assess the catalytic activity of purified Polκ wildtype (WT) and mutants, 1 μM of primer 30 (105 nt) and 0.25 μM of fluorescently labelled primer 31 (35 nt) were mixed in 20 mM HEPES-KOH (pH 7.5) and 50 mM KAc, incubated at 95°C for 5 min, and allowed to reach RT. DNA ends were blocked with a four-fold excess of monovalent streptavidin (SAE0094, Sigma–Aldrich) for 30 min at RT. All experiments were performed at RT in 25 mM HEPES-KOH (pH 7.5), 150 mM KAc, 8 mM $MgAc_2$, 1 mM TCEP, 1 mM ATP, and 0.2 mg/ml bovine serum albumin. The concentrations reported below refer to the final reactions. DNA with blocked ends (25 nM) was incubated with RPA (75 nM) for 5 min. Subsequently, PCNA (150 nM trimer) and RFC (15 nM) were added and incubated for 10 min. After which, Polκ (50 nM) with dNTPs (100 μM each) was added, starting DNA synthesis. One volume of denaturing PAGE Gel Loading Buffer II (Invitrogen™) was added to stop reactions. Samples were denatured by incubation at 98°C for 5 min and immediately loaded on 20% PAGE containing 7M urea. Human PCNA and PCNA-ub used for this experiment were purified as previously reported [63], and yeast RFC and RPA were purified as previously reported [64].

Results

Preparation of acrolein interstrand crosslink-containing plasmids

AA-ICLs are repaired by the FA pathway and an excision-independent pathway [19]. To determine whether this also applies to other aldehyde-ICLs, we generated a DNA substrate containing an acrolein interstrand crosslink (ACR-ICL) (Supplementary Fig. S1A–D). Acrolein reacts with the N_2 of guanine, creating the precursor γ-OH-N_2-propanoguanine (γ-OH-PdG), generating a stable ring-closed adduct in single-stranded DNA that opens when paired with a cytosine in duplex DNA [21, 22, 65, 66]. In this open conformation, the γ-position aldehyde can react with the N^2 of a guanine in the opposing strand when in a 5′-CpG-3′ context [19, 67], creating a duplex containing a native acrolein ICL (ACR_{NAT}-ICL) (Fig. 1A). Like native acetaldehyde ICLs (AA_{NAT}-ICL), ACR_{NAT}-ICLs exist in an equilibrium of the carbinolamine, imino, and pyrimidopurone species (Fig. 1A) [19–23, 66, 67]. ACR_{NAT}-ICL-containing oligo duplexes were chemically generated and ligated into a plasmid backbone [49], creating pICL-ACR_{NAT} (Supplementary Fig. S1E). We also generated a non-reversible reduced ACR-ICL in pICL-ACR_{RED}, in an almost identical sequence context. Both native and reduced acrolein ICLs were stable upon incubation in *Xenopus* egg extract at RT and neutral pH (Supplementary Fig. S1F). While the native ACR-ICL reversed upon exposure to acidic conditions, consistent with protonation of the 2′-deoxyguanosine (dG) N^2-amino group followed by Schiff-base hydrolysis, the reduced ACR-ICL was stable under these conditions as expected (Supplementary Fig. S1D). We also generated the non-damaged pCtrl-ACR with the same sequence as pICL-ACR_{RED} and the mono-adducted γ-OH-PdG (pMono-ACR) and Me-γ-OH-PdG (pMono-AA) containing plasmids, as well as cisplatin and acetaldehyde ICL-containing plasmids (pICL-Pt, pICL-AA_{NAT}, and pICL-AA_{RED}) [19, 49]. All aldehyde lesions investigated affect the minor groove, while cisplatin-ICLs affect the major groove of the DNA.

Acrolein ICLs are repaired by two pathways

We previously described that Pt- and AA_{RED}-ICLs are repaired by the FA pathway during DNA replication in *Xenopus* egg extract [19]. Replication of these plasmids in extract, and separation of the reaction products on native agarose gel, generates a characteristic FA pathway pattern of Replication and Repair Intermediates (RRI), including a ‘figure 8’ structure upon replication fork convergence, followed by low mobility HR intermediates and fully resolved nicked and supercoiled (SC) products at later times (Supplementary Figs S1H and S2A). Analysis of replication products of pICL-ACR_{NAT} resulted in the accumulation of both the characteristic FA RRI pattern as well as a faster and more prominent increase in the open circular (OC) and SC products, similar to our previous observations for pICL-AA_{NAT} [19] (Supplementary Fig. S2A). This suggests that pICL-ACR_{NAT}, like pICL-AA_{NAT}, is repaired by the FA pathway and a faster repair pathway. Consistent with this, addition of a p97 segregase inhibitor (p97i) that prevents unloading of the CMG helicase, an essential step in the FA pathway [51, 68], induced partial replication fork stalling visualized by an accumulation of converged forks (Supplementary Fig. S2B). Replication of pICL-ACR_{RED} in the presence of p97i induced complete replication stalling, indicating repair fully relies on the FA pathway. Furthermore, we monitored repair directly using the previously described NotI assay [19] (Supplementary Fig. S2C). As expected, inhibition of the FA pathway by p97i completely prevented the formation of repair products upon replication of pICL-AA_{RED}, pICL-ACR_{RED}, and pICL-Pt (Fig. 1B and C and Supplementary Fig. S2D). In contrast, the addition of p97i only partially inhibited the repair of both pICL-

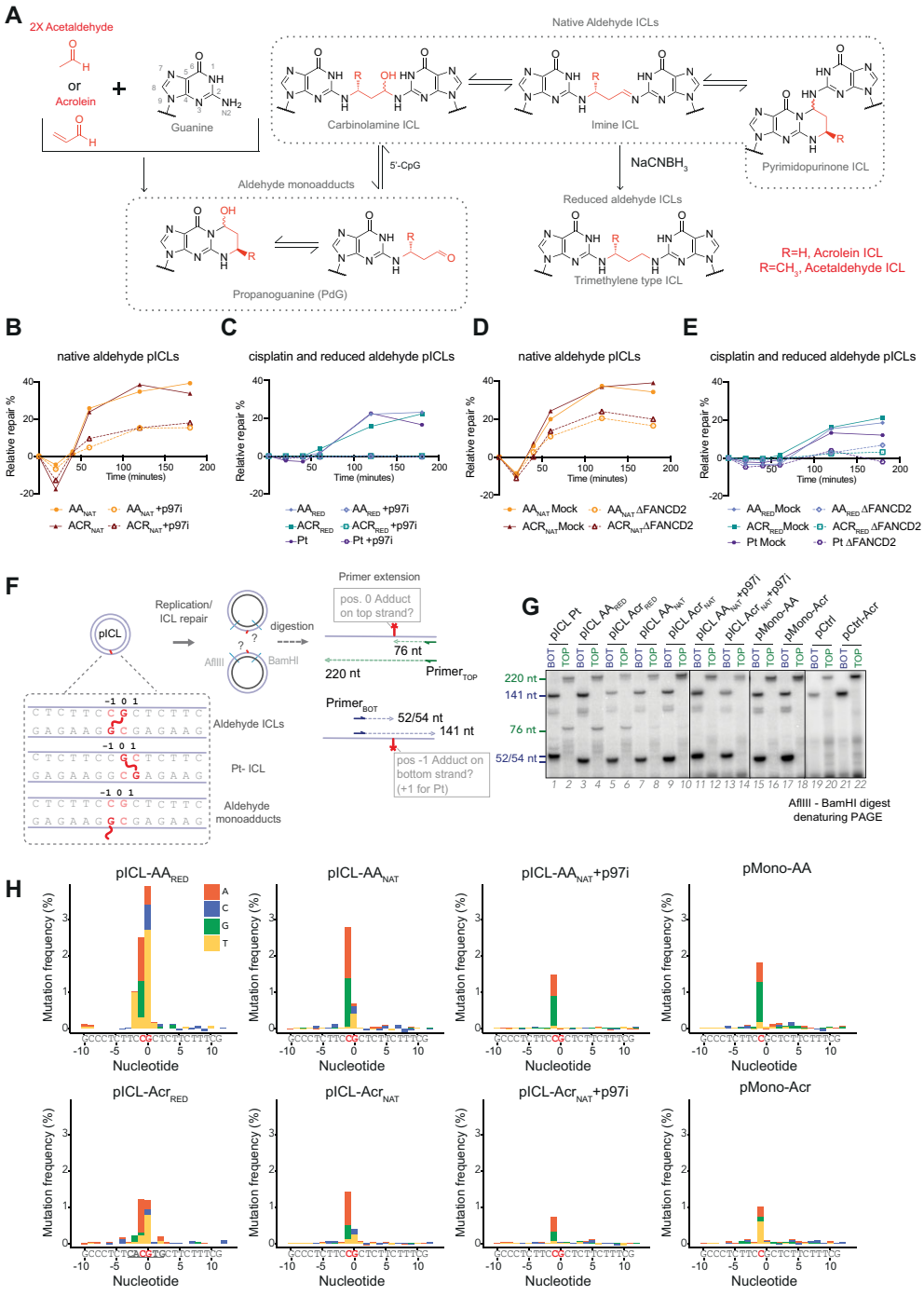

Figure 1. Acrolein ICLs are repaired via the FA and excision-independent pathway. (**A**) Reaction scheme of the formation of native and reduced aldehyde-ICLs: two acetaldehyde or one acrolein molecules react with a guanine in a DNA strand to form mono-adducts. This reacts with a 5′CpG guanine on the opposite strand. The resulting native aldehyde-ICLs exist in an equilibrium between three forms. The crosslink can be chemically reduced with sodium cyanoborohydride to form reduced aldehyde ICLs, which can also be generated by alternative methods (see the 'Materials and methods' section). (**B**) Quantification of repair of native acrolein and acetaldehyde ICLs (ACR_{NAT}-ICL, AA_{NAT}-ICL) in p97i-treated extract, based on gels in Supplementary Fig. S2D. (**C**) Quantification of repair of reduced acrolein (ACR_{RED}-ICL), reduced acetaldehyde (AA_{RED}-ICL), and Cisplatin ICLs (Pt-ICL) in p97i treated extract, based on gels in Supplementary Fig. S2D. (**D**) Quantification of repair of ACR_{NAT}-ICL and AA_{NAT}-ICL in mock and FANCD2-depleted extract, based on gels in Supplementary Fig. S2F. (**E**) Quantification of repair of ACR_{RED}-ICL, AA_{RED}-ICL, and Pt-ICL in mock and FANCD2-depleted extract, based on gels in Supplementary Fig. S2F. (**F**) Scheme of the *in vitro* primer extension assay. Late replication and repair products are extracted, digested with AflIII and BamHI, and used as templates for primer extension from radioactively labelled top-strand (TOP) and bottom-strand (BOT) primers. Non-adducted strands will generate full-length extension products (220 or 141 nt), while adducted strands will stall extension and generate shorter products (52 nt for Aldehyde-ICL and 54 nt for Pt-ICL). (**G**) Primer extension products are separated on 20% urea–PAGE gels and visualized by autoradiography. (**H**) Distribution and frequency of nucleotide misincorporation in a 20-bp region containing the indicated lesions (method details in Supplementary Fig. S3C) of late replication products of indicated plasmids. pICL-AA_{NAT} was replicated in the presence of p97i or DMSO for comparison. Positions of crosslinked nucleotides are indicated in red. pICL-ACR_{RED} has a 6-nt sequence difference (−2 to +3, underlined) from the other plasmids. Distributions of mutation types (deletions, SNVs, and WT) are indicated in Supplementary Fig. S3D. Non-damaged plasmids did not accumulate mutations (Supplementary Fig. S3E).

AA_{NAT} and pICL-ACR_{NAT}, indicating an FA-independent repair mechanism is active on these plasmids. Finally, depletion of FANCD2 [15] further confirmed the role of the FA pathway in ACR_{NAT}-ICL and ACR_{RED}-ICL repair (Fig. 1D and E and Supplementary Fig. S2F).

The excision-independent pathway repairs AA_{NAT}-ICLs and ACR_{NAT}-ICLs

Similar to the repair of AA_{NAT}-ICLs [19], the FA-independent route of ACR_{NAT}-ICL repair did not involve ICL unhooking by DNA backbone incisions or cleavage of the *N*-glycosyl bond (Supplementary Fig. S3A and B). We next examined adduct formation after ICL unhooking by performing primer extension reactions with high-fidelity polymerase on late replication products (Fig. 1F). We previously showed that ICL repair by the FA pathway generates an adduct on the top or bottom strand, while the excision-independent repair pathway only generates an adduct on the bottom strand [19]. Consistently, primer extension on repair products of pICL-Pt, pICL-AA_{RED}, and pICL-ACR_{RED} was stalled on both the top and bottom strands (Fig. 1G, lanes 1–6). Repair products of pICL-AA_{NAT} and pICL-ACR_{NAT} showed prominent stalling of primer extension on the bottom strand, similar to pMono-AA and pMono-ACR products, but also generated mild stalling products at the top strand (Fig. 1G, compare lanes 7–10 to lanes 15–18). Upon blocking the FA pathway, top strand stalling products were lost, indicating that the second pathway of pICL-ACR_{NAT} repair only generates a polymerase blocking adduct on the bottom strand (Fig. 1G, compare lanes 7–10 to lanes 11–14).

To investigate the mutagenicity of the bypass of these adducts, we sequenced late repair products (Supplementary Fig. S3C). FA pathway-mediated repair of the reduced aldehyde ICLs induced mutations mostly at the positions of the crosslinked guanines (positions −1 and 0) [19] (Fig. 1H). ACR_{NAT}-ICL repair products also showed mutations at the −1 and 0 positions, and similar to what we observed for AA_{NAT}-ICL repair, FA-pathway inhibition eliminated mutations at position 0 [19] (Fig. 1H). The remaining mutations at the position of the bottom strand guanine are very similar to mutations induced by replication of pMono-ACR, although interestingly, the mutation pattern is different. This indicates that the excision-independent pathway creates an adduct on the bottom strand that may not be identical to the adduct in pMono-ACR. Furthermore, FA-mediated repair activity contributes to an increase in deletions compared to excision-independent repair, consistent with double-strand break formation in the FA pathway (Supplementary Fig. S3D).

In conclusion, these results show that both AA_{NAT}-ICLs and ACR_{NAT}-ICLs, in addition to being repaired by the FA pathway, are also repaired by the excision-independent pathway, indicating a general aldehyde-ICL repair strategy.

Rev1–Polζ promotes insertion for aldehyde ICLs but extension for cisplatin ICLs

DNA synthesis past the unhooked adduct during ICL repair requires specialized TLS polymerases. The TLS complex Rev1–Polζ plays a role in both Pt-ICL and AA-ICL repair but acts in a different step; depletion of Rev1–Polζ generates a defect in insertion in AA-ICLs, while it inhibits extension in Pt-ICLs [17, 19]. To examine the role of Rev1–Polζ in ACR-ICL repair, we monitored lesion bypass in extract depleted of Rev1, which co-depletes Polζ, by analysing the nascent strands of pICL-ACR_{NAT} and pICL-ACR_{RED} repair products on a sequencing gel. Stalling at the −1 position, 1 nt before the ICL, was moderately enhanced in the absence of Rev1 compared to the mock (Supplementary Fig. S4B, compare lanes 21 and 22 to lanes 26 and 27, and lanes 30 and 31 to lanes 35 and 36), indicating the insertion step was affected in both pICL-ACR_{NAT} and pICL-ACR_{RED} repair. However, the Rev1–Polζ depletion defect in lesion bypass was mild compared to pICL-Pt for the reduced acrolein (Supplementary Fig. S4B, compare lanes 3 and 4 to 8 and 9, and lanes 30 and 31 to 35 and 36), as well as the reduced acetaldehyde [19] ICLs that entirely depend on the FA pathway. This is consistent with previous reports showing that cells deficient in Rev1 are only mildly sensitive to acetaldehyde [8–10] and suggests that another TLS polymerase may be more critical in aldehyde ICL repair.

Polκ promotes TLS during aldehyde-ICL repair

To identify other TLS polymerases involved in aldehyde ICL repair, we pulled down ICL-containing plasmids during repair in extract and analysed plasmid-bound proteins by mass spectrometry (pp-ms) (Fig. 2A). As expected, we detected Rev1 and Polζ on both pICL-Pt and pICL-AA_{NAT}. Furthermore, we observed an enrichment of another TLS polymerase, Polκ, especially on pICL-AA_{NAT} (Fig. 2B and Supplementary Table S1). Interestingly, Polκ-deficient cells are sensitive to ICL-inducing agents causing N2–N2 guanine crosslinks, such as Mitomycin C [69–71]. We generated antibodies against an N-terminal and C-terminal peptide of *Xenopus laevis* Polκ. The C-terminal antibody efficiently depleted Polκ from extract and, importantly, does not co-deplete Rev1 or Polζ (Fig. 2C). We decided to focus on the FA pathway branch of repair because the unhooked adduct, which is the substrate for TLS, is well-defined in this pathway. Moreover, the reduced version of this ICL enables selective FA pathway readout. Therefore, we replicated pICL-AA_{RED} in mock and Polκ-depleted extract and separated replication intermediates on a native agarose gel (Supplementary Fig. S4E). While early replication intermediates (figure 8-structures) accumulated with similar kinetics, OC products generated by ICL unhooking persisted in the absence of Polκ, and the accumulation of SC products was delayed, indicative of a defect in TLS. This defect was further exacerbated upon Polκ–Rev1 double depletion. Next, we analysed lesion bypass at higher resolution on sequencing gels (Fig. 2D and E). Polκ depletion induced a persistent stalling at the −1 position that was more pronounced compared to a Rev1-depleted extract (Fig. 2E, compare lanes 5 and 6 to lanes 11 and 12, and 17 and 18). While single depletion of Rev1 had only a mild effect on lesion bypass, double depletion of both Polκ and Rev1 further enhanced −1 stalling and blocked the accumulation of insertion products (0 position) (Fig. 2E, compare lanes 5 and 6 to lanes 17 and 18, and 23 and 24). We observed a similar TLS defect for pICL-ACR_{RED} upon Polκ and Rev1 depletion (Supplementary Fig. S4C, compare lanes 4–6 to lanes 10–12 and lanes 16–18, and Supplementary Fig. S4F), suggesting Polκ plays a key role in the insertion step during aldehyde ICL repair by the FA pathway. In contrast, replicating pICL-Pt in a Polκ-depleted extract caused only mild stalling at the 0-position, indicative of a defect in extension, similar to a Rev1-depleted extract (Supplementary Fig. S4D and G). This suggests Polκ and Rev1 act in different steps of

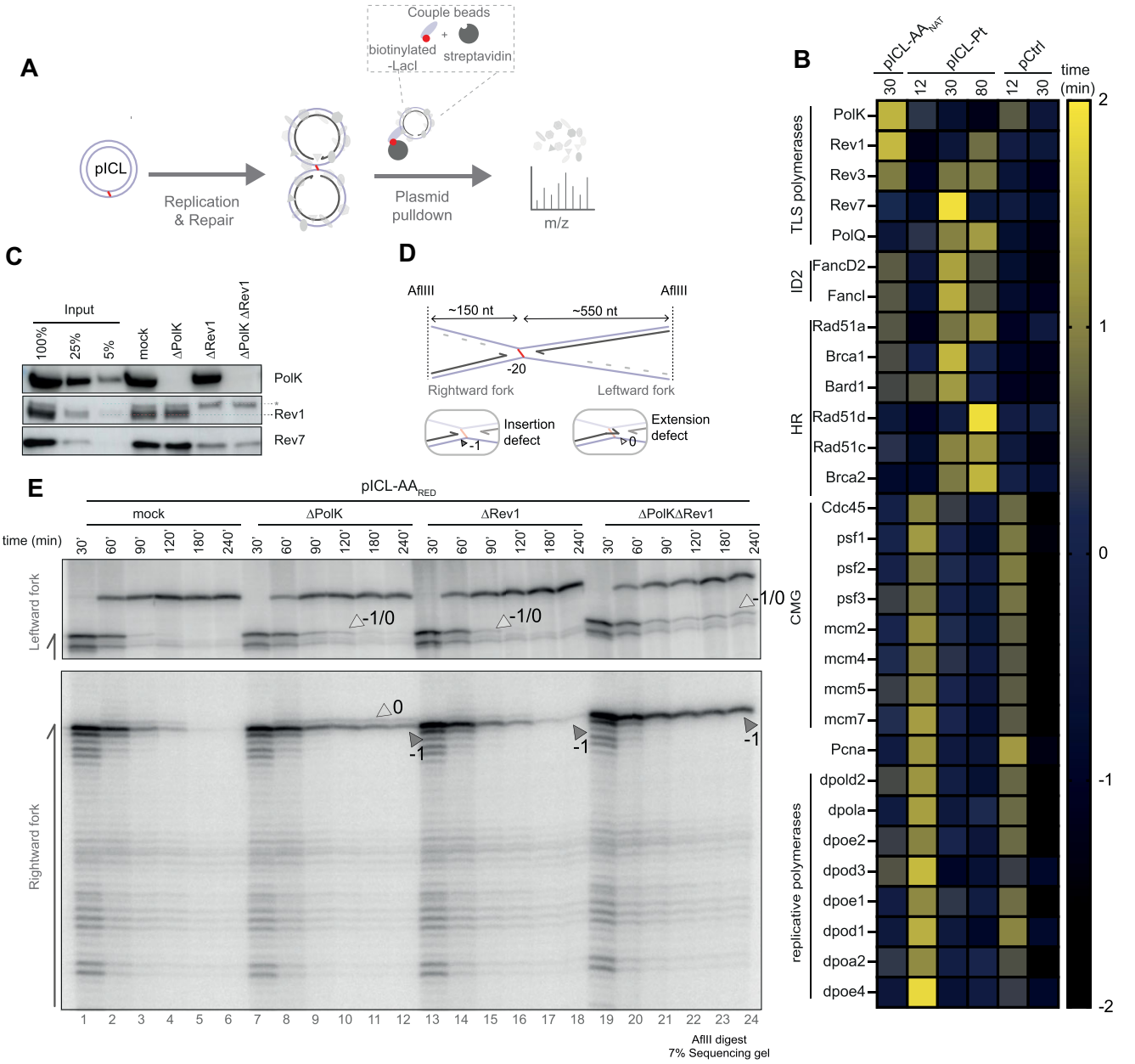

Figure 2. Polκ acts in FA pathway-mediated TLS during aldehyde-ICL repair. (**A**) Scheme of plasmid pulldown assay coupled to mass spectrometry (pp-ms). Biotinylated LacI-coupled streptavidin beads are used to pull down reaction intermediates during ICL repair. DNA-bound proteins are identified by MS analysis. (**B**) Relative abundance of indicated proteins is represented by a heatmap showing *Z*-scores (mean from four biological replicates). (**C**) Western blot analysis of mock, Polκ, Rev1, or Polκ/Rev1 depleted egg extract alongside a titration of undepleted extract. (**D**) Scheme for the formation of products detected on a sequencing gel, nascent products in grey. (**E**) Repair intermediates of pICL-AA$_{RED}$ replicated in mock, Polκ, Rev1, or Polκ/Rev1 depleted egg extract supplemented with ^{32}P-dCTP are extracted, digested with AflIII, and separated on a 7% urea–PAGE gel. Grey arrows: −1 stalling products; open arrows: 0 stalling products; white arrows: −1/0 stalling products.

TLS; they promote insertion during aldehyde ICL repair and extension during repair of cisplatin ICLs.

Differential role of Polκ in bypass of aldehyde-ICL versus cisplatin-ICL adducts

To validate that Polκ directly acts in TLS of aldehyde ICL repair by the FA pathway, we purified recombinant *Xenopus laevis* Polκ expressed in *Spodoptera frugiperda* (Sf9) cells (Supplementary Fig. S6A). Addition of purified Polκ to a Polκ-depleted extract (Fig. 3A) fully rescued the insertion defects during pICL-ACR$_{RED}$ and pICL-AA$_{RED}$ repair (Fig. 3B, compare lanes 7 and 8 to lanes 11 and 12, and lanes 19 and 20 to lanes 23 and 24) and also the milder extension defect during pICL-Pt repair (Fig. 3B, compare lanes 31 and 32 to lanes 35 and 36). Consistently, recombinant Polκ also fully rescued the formation of SC products as visualized on native agarose gel (Supplementary Fig. S5A–C, quantified in Supplementary Fig. S5D–F).

To monitor lesion bypass during FA pathway-mediated repair more quantitatively, we employed a lesion bypass assay that involves linearization of replication products followed by separation on a denaturing agarose gel to visualize nascent strands (Fig. 3C). Full-length linear products accumulate over

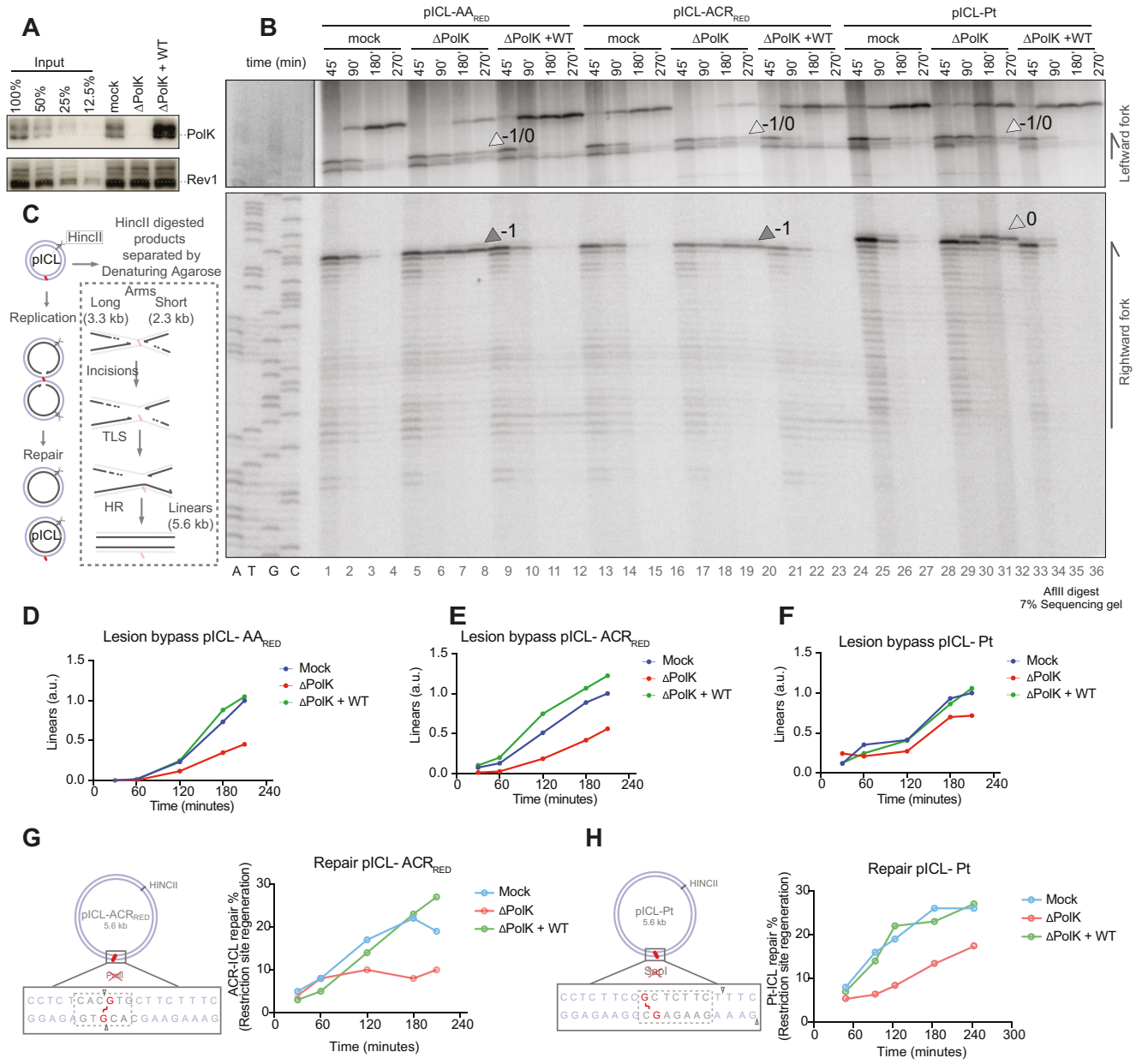

Figure 3. Polκ promotes insertion for aldehyde ICLs and extension for cisplatin ICLs. (**A**) Western blot analysis of mock, Polκ-depleted (ΔPolκ), and Polκ-depleted egg extract supplemented with recombinant WT Polκ (ΔPolκ + WT), alongside a titration of undepleted extract. (**B**) Repair intermediates of pICL-AA$_{RED}$, pICL-ACR$_{RED}$, and pICL-Pt replicated in mock, ΔPolκ, and ΔPolκ + WT egg extract supplemented with ^{32}P-dCTP were extracted, digested with AflIII, and separated on a 7% urea–PAGE gel. Grey arrows: −1 stalling products; open arrows: 0 stalling products; white arrows: −1/0 stalling products. The stalled products of the rightward fork at Pt-ICLs are 2 nt longer compared to the aldehyde ICLs due to a difference in ICL position as described in Fig. 1F. (**C**) Schematic representation of the lesion bypass assay. Replication/repair intermediates are digested with HincII and separated on a denaturing agarose gel. Long and short arms appear as the replication forks approach the lesion and are converted to full-length products following TLS and HR. An undamaged plasmid (pQuant) is added to the reactions for quantification. Quantification of lesion bypass assays on pICL-AA$_{RED}$ (**D**), pICL-ACR$_{RED}$ (**E**), and pICL-Pt (**F**) repair reactions in mock, ΔPolκ, and ΔPolκ + WT egg extract. Based on gels in Supplementary Fig. S5G–I. (**G**) Repair intermediates of pICL-ACR$_{RED}$ replication reactions in mock, ΔPolκ, and ΔPolκ + WT egg extracts were digested with HincII, or HincII and PmlI, and separated on agarose gel (Supplementary Fig. S5J). Repair was calculated based on the regeneration of the PmlI recognition site (left scheme) and plotted (right). (**H**) Similar to (G) but for pICL-Pt, containing a SapI restriction site (left scheme) that is regenerated upon repair. Based on gel in Supplementary Fig. S5K.

time, which represent TLS products and subsequent DSB repair products of the incised strand. A smaller non-damaged plasmid (pQuant) was added to each reaction for normalization, allowing full-length product quantification. Using this assay, we show that Polκ depletion reduced linear products down to 50% in pICL-AA_{RED} and pICL-ACR_{RED} repair, suggesting a strong inhibition of TLS, while the linear products of Pt-ICLs were only reduced to 70% (Fig. 3D–F and Supplementary Fig. S5 G–I). The addition of recombinant Polκ fully rescued formation of full-length products in all plasmids.

Finally, we monitored faithful repair via restriction site regeneration for pICL-ACR_{RED} and pICL-Pt. Consistent with the TLS results, we found Polκ depletion greatly reduced ACR_{RED}-ICL repair (Fig. 3G and Supplementary Fig. S5J), while it had a milder effect on Pt-ICL repair (Fig. 3H and Supplementary Fig. S5K). The addition of recombinant Polκ fully rescued both defects. In conclusion, Polκ acts directly in the insertion step of TLS across unhooked aldehyde ICLs and in the extension step across unhooked Pt-ICLs in the FA pathway, promoting faithful repair.

Polκ-mediated insertion across unhooked aldehyde ICLs depends on its catalytic and PCNA-interacting domains

To identify which functional domains of Polκ contribute to its role in lesion bypass in the FA pathway, we purified Polκ carrying point mutations in the catalytic domain (CD), the Rev1 interaction region (RIR), both PCNA interaction peptides (PIP1 and PIP2), or both the ubiquitin-binding zinc fingers (UBZ1 and UBZ2) [42, 71–74] (Fig. 4A and Supplementary Fig. S6A). We examined the polymerase activity of WT and mutant recombinant proteins in an *in vitro* primer extension assay (Supplementary Fig. S6B and C) in the presence and absence of PCNA. Consistent with human Polκ [42, 75], the polymerase activity of *Xenopus laevis* Polκ was greatly enhanced in the presence of PCNA (Supplementary Fig. S6C, compare lane 1 to lane 4), and consequently, mutation of the PIPs inhibited primer extension (Supplementary Fig. S6C, compare lane 4 to lane 12). The CD mutant was also defective in primer extension, while the RIR and UBZ mutants extended the primer as efficiently as WT Polκ (Supplementary Fig. S6C, compare lane 4 to lanes 8, 16, and 20). We then added the Polκ mutants to Polκ-depleted egg extract (Fig. 4B) and analysed lesion bypass during ICL repair. The CD and PIP mutants did not rescue the −1-stalling induced by Polκ depletion during pICL-ACR_{RED} repair (Fig. 4C, compare lanes 16–20 and 26–30 to 11–15). The lack of rescue by these mutants during aldehyde ICL repair was further confirmed in the quantitative lesion bypass assay (Fig. 4D and E and Supplementary Fig. S7A and B) and was also evident by the persistence of OC products on native gels (Supplementary Fig. S7C–F). Interestingly, the interaction between Polκ and Rev1 was not required, because the −1 stalling was fully rescued upon addition of the RIR mutant (Fig. 4C compares lanes 21–25 to lanes 11–15), full-length products were efficiently generated (Fig. 4D and E and Supplementary Fig. S7A and B), and SC products accumulated similarly to WT protein addition (Supplementary Fig. S7C–F). Finally, the UBZ mutant showed an intermediate effect; it partially rescued the −1 stalling (Fig. 4C, compare lanes 31–35 to lanes 11–15), the generation of full-length products, and the OC to SC conversion (Fig. 4D and E, and Supplementary Fig. S7C–F). The UBZ domains of Polκ could interact with ubiquitylated PCNA. PCNA is ubiquitylated and PCNA-Ub is bound to the plasmid during aldehyde ICL repair (Supplementary Fig. S6D and E). To examine whether PCNA ubiquitylation could affect Polκ activity by interaction with the UBZ domains, we performed a primer extension assay with PCNA-Ub. However, PCNA-Ub did not enhance primer extension by Polκ compared to PCNA (Supplementary Fig. S6F, compare lane 8 to lane 12), indicating this interaction does not affect Polκ's activity directly. Together, this data indicates that Polκ-mediated TLS during aldehyde ICL repair by the FA pathway depends on its catalytic activity and PCNA interaction, while interaction with Rev1 is not required and the UBZ domains play at most an accessory role.

Polκ promotes Rev1–polζ-mediated extension in a non-catalytic manner during cisplatin ICL repair

We also observed a mild lesion bypass defect during the repair of pICL-Pt upon Polκ depletion. In contrast to the aldehyde ICLs, this defect was largely rescued by the CD, PIP, and UBZ domain mutants. However, the RIR mutant did not rescue the defect (Fig. 4F and Supplementary Fig. S8A–C). Consistently, the RIR mutant did not rescue the −1-stalling visualized on a sequencing gel, while the CD mutant did (Supplementary Fig. S8D, compare lanes 14 and 15 to lanes 19 and 20 and lanes 24 and 25). This finding indicates that Polκ has a non-catalytic function dependent on Rev1 interaction in the extension step of cisplatin ICL repair. This is in line with the recently described supporting function of Polκ to Rev1–Polζ in major groove adducts [31].

Polκ is recruited independently of Rev1 during aldehyde ICL repair by the FA pathway

While Rev1 and Polζ are both recruited to aldehyde ICLs during repair (Fig. 2B), and Rev1 depletion in addition to Polκ depletion enhances TLS stalling compared to single Polκ depletion (Fig. 2E and Supplementary Fig. S4D), the interaction between Rev1 and Polκ is dispensable for TLS during FA-pathway-mediated repair (Fig. 4C). This suggests that Polκ is not recruited to the lesion via Rev1 but rather that they act independently. To investigate the functional relationship between Rev1 and Polκ further, we depleted both proteins from egg extract and monitored linear product formation upon adding Polκ WT and mutants (Fig. 5A). Addition of Polκ WT to the double depleted extract rescued the defect to about 80% compared to the mock depleted extract during pICL-AA_{red} (Fig. 5B and Supplementary Fig. S9A, C, and D) and pICL-ACR_{red} (Fig. 5C and Supplementary Fig. S9B, E, and F) repair. This shows that Polκ can promote lesion bypass independently of the presence of Rev1 and its scaffolding function. Moreover, the Rev1 interaction mutant rescued the generation of full-length products equally to the WT protein. Lesion bypass by the recombinant WT or RIR mutant Polκ did not fully rescue the effect compared to the levels in the mock condition. This is consistent with the additive effect of Rev1 and Polκ double depletion compared to Polκ single depletion as seen in Fig. 2E, indicating Rev1–Polζ can promote some TLS independently of Polκ. As also observed upon Polκ depletion (Fig. 4C–E and Supplementary Fig. S7A–F), in the double-depleted

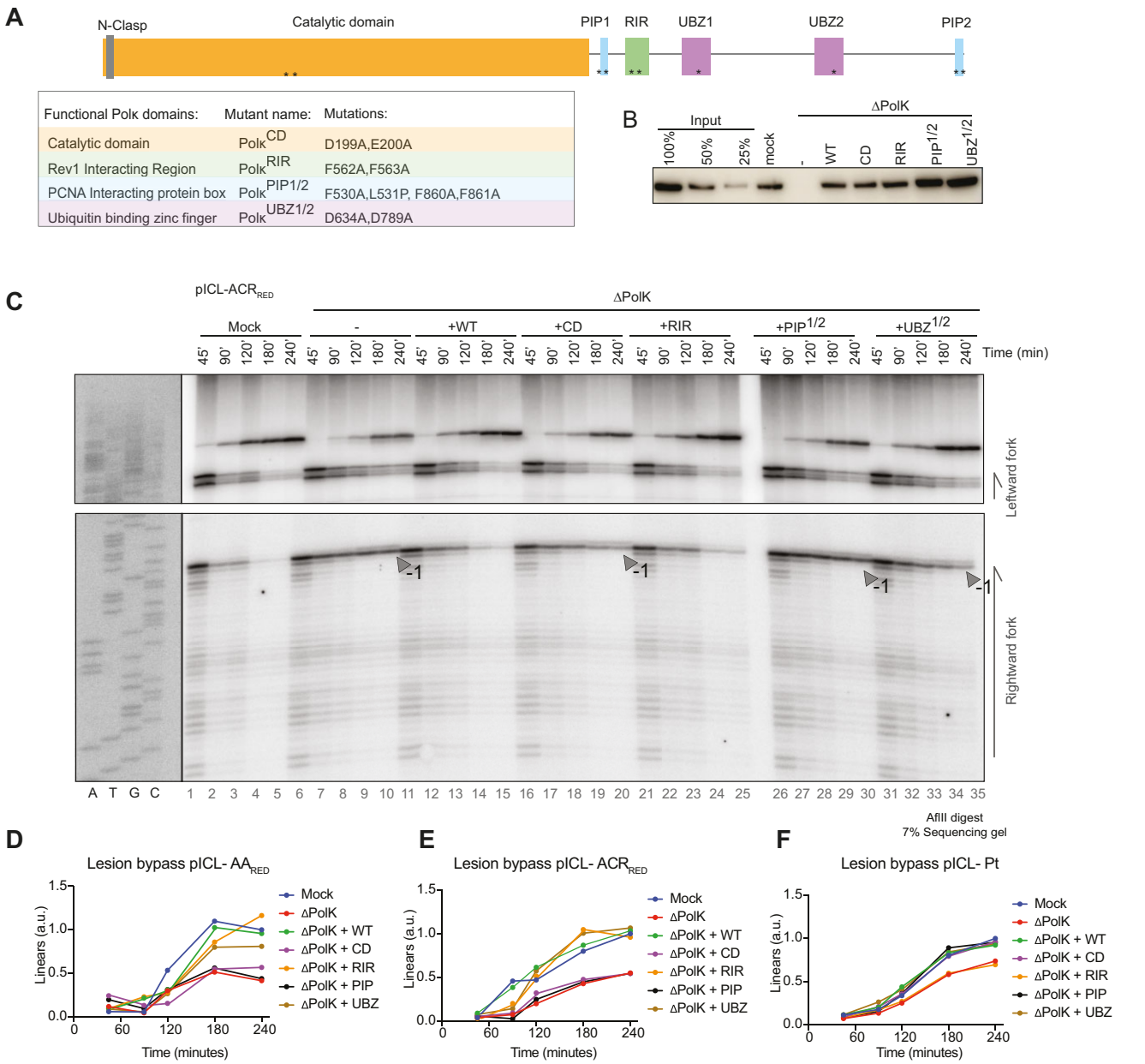

Figure 4. Polκ-PCNA interaction and its CDs are important for insertion during FA-mediated aldehyde ICL repair. (**A**) Schematic representation of *x*/Polκ indicating its functional domains. Mutations are indicated and described in the table (bottom). (**B**) Western blot analysis of mock, Polκ-depleted (ΔPolκ), and Polκ-depleted egg extract supplemented with WT Polκ or mutants, alongside a titration of undepleted extract. (**C**) Repair intermediates of pICL-ACR$_{RED}$ replicated in mock, ΔPolκ, and ΔPolκ egg extract supplemented with WT or indicated mutant Polκ were extracted, digested with AflIII, and separated on a 7% urea–PAGE gel. Grey arrows: −1 stalling products. Quantifications of lesion bypass assays on pICL-AA$_{RED}$ (**D**), pICL-ACR$_{RED}$ (**E**), and pICL-Pt (**F**) repair reactions in mock, ΔPolκ, and ΔPolκ + WT or mutant Polκ extract. Based on gels in Supplementary Figs S7A and B, and S8A.

extract the CD and PIP mutants did not rescue TLS. Additionally, these data show that Rev1–Polζ is not required for the extension step, which, in its absence, is probably performed by Polκ, consistent with previous reports that Polκ can carry out extension during TLS [76, 77]. Whether Polκ or Rev1–Polζ promotes extension in non-depleted conditions remains to be determined.

Polκ-mediated bypass during aldehyde ICL repair by the FA pathway is mostly faithful

Repair of aldehyde ICLs via the FA pathway is mutagenic, as observed in Fig. 1H. To determine the contribution of Polκ and Rev1 to the mutational load, we sequenced pICL-AA$_{RED}$ repair products from Rev1- and Polκ-depleted extracts. While more deletion products were detected in all depleted compared to non-depleted conditions (compare Supplementary Fig. S3D with Supplementary Fig. S10A and B and [17]), a further increase in deletion products was specifically detected upon Polκ depletion in two independent experiments (Supplementary Fig. S10A and B). This is consistent with Polκ being the primary TLS polymerase because compromised lesion bypass reduces the availability of the HR template, thereby favouring end joining-inducing deletions.

SNV analysis showed the misincorporation pattern in the mock depleted extract was very similar to the undepleted extract (compare Figs. 1H and 5D). Unexpectedly, depletion of

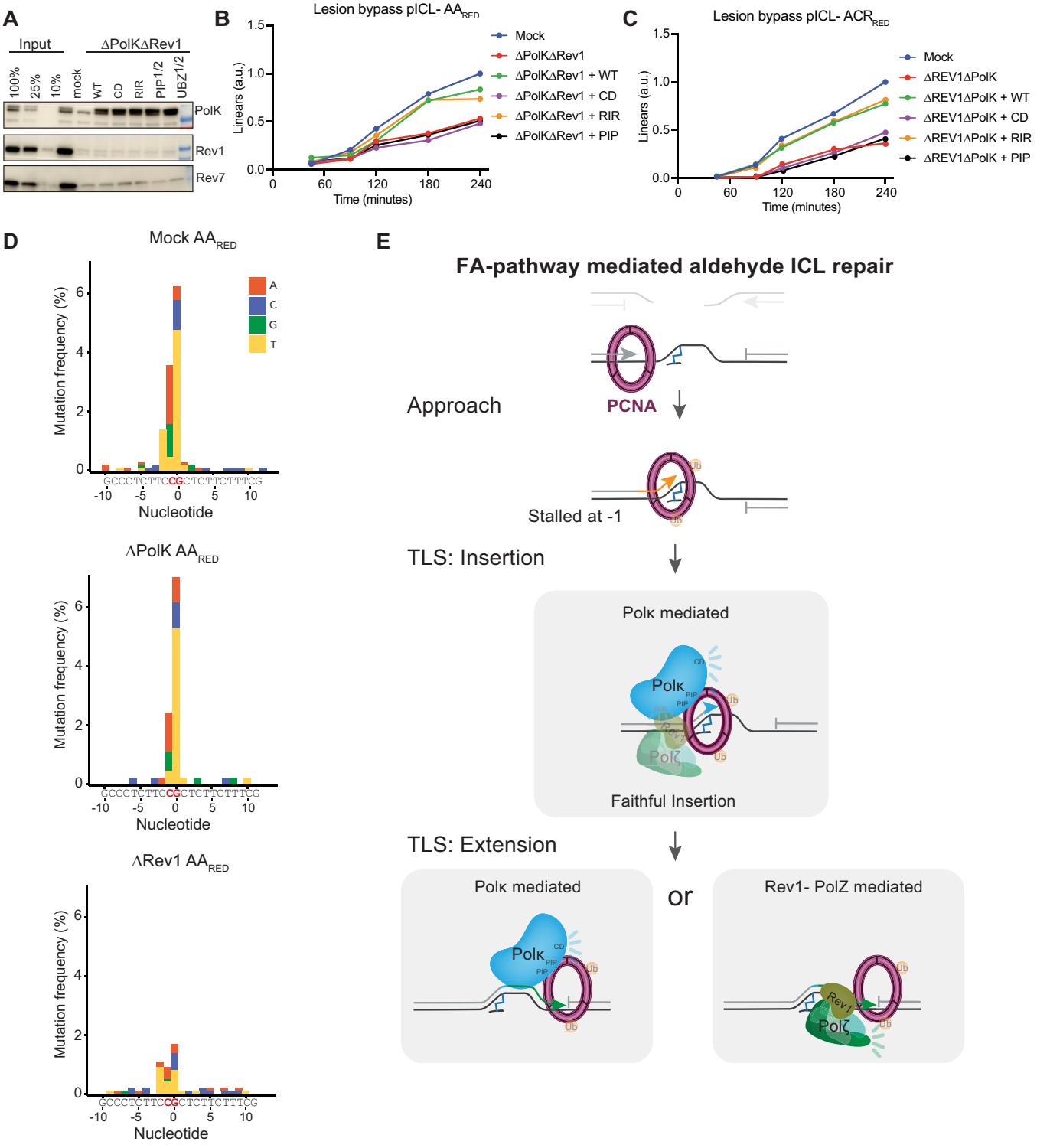

Figure 5. Polκ mediates faithful bypass of unhooked aldehyde ICLs, independently of Rev1. (**A**) Western blot analysis of mock, Polκ and Rev1 (ΔPolκΔRev1) depleted extract, and ΔPolκ ΔRev1 extract supplemented with the indicated WT or mutant Polκ proteins alongside a titration of undepleted extract. (**B**, **C**) Quantifications of lesion bypass assays on pICL-AA_{RED} (**D**) and pICL-ACR_{RED} (**E**) repair reactions in mock, ΔPolκ ΔRev1 double depleted extract, and ΔPolκΔRev1 extract supplemented with indicated Polκ WT or mutant proteins. Based on gels in Supplementary Fig. S9C and D. (D) Distribution and frequency of nucleotide misincorporation of pICL-AA_{RED} repair products from Mock, Rev1, or Polκ depleted extract. Distributions of all mutation types (deletions, SNVs, and WT) are indicated in Supplementary Fig. S10A. (E) Model of the role of Polκ in aldehyde-ICL repair via the FA pathway. Polκ is the main insertion polymerase for unhooked aldehyde-ICL adducts during FA-mediated repair. For this, Polκ depends on its PIP domains and catalytic activity. The extension step is performed by either Rev1–Polζ or Polκ, which likely both are present at the lesion.

Polκ did not cause a major change in the misincorporation pattern or rate, which suggests that these are not caused by Polκ (Fig. 5D and Supplementary Fig. S10C). This is consistent with previous reports indicating Polκ TLS is relatively error-free [44, 78–80]. In contrast, Rev1 depletion reduced the mutation rate and changed the mutation pattern, indicating that the small fraction of adducts that require Rev1 for lesion bypass during AA_{RED}-ICL repair are responsible for inducing the majority of the observed misincorporations in undepleted conditions. Because Rev1's catalytic activity is restricted to insertion of cytosines, which would not cause mutations across from adducted guanines, this indicates possible involvement of another mutagenic polymerase. This redundant polymerase could be Polη or Polθ, as they are recruited to the aldehyde-ICL plasmids in mock-depleted extracts as well as in extracts depleted of Polκ or Rev1 (Supplementary Fig. S10D).

Together, our results support a model in which Polκ is the primary insertion polymerase during aldehyde ICL repair by the FA pathway that bypasses adducts relatively error-free (Fig. 5E). In a small fraction of lesions, as well as in the absence of Polκ, Rev1–Polζ promotes insertion, likely mediated by a different mutagenic polymerase. Extension can be carried out by both Rev1–Polζ and Polκ (Fig. 5E).

Discussion

While most of our understanding of the mechanism of ICL repair has resulted from investigating ICLs induced by chemotherapeutic agents, less is known about the repair mechanisms of endogenous ICLs. Using *Xenopus* egg extracts, we show that not only acetaldehyde but also acrolein-induced ICLs are repaired by two pathways: the FA pathway and the excision-independent pathway, providing evidence for a general aldehyde ICL repair strategy. It is probable that these mechanisms therefore also extend to repair of 1,N^2-dG exocyclic products, such as *trans*-4-hydroxynonenal (4-HNE), generated from cellular processes such as lipid peroxidation [21]. Focusing on the FA-pathway branch, we identify Polκ as the primary TLS polymerase responsible for faithful insertion during lesion bypass. We determined key requirements for Polκ function during this process and showed how different ICL lesions use different mechanisms of TLS.

Polκ has been shown to promote TLS via a catalytic and non-catalytic mechanism depending on the lesion position in the minor or major groove [31]. Consistent with this study, we show that the CD is important to promote the insertion step of TLS during the repair of minor groove aldehyde ICLs by the FA pathway. While this previous study reported TLS was independent of Rev1, from our experiments we currently cannot definitively conclude whether the extension step is performed by Polκ or Rev1–Polζ. We have previously shown that Rev1 is important for TLS past acetaldehyde mono-adducts [19], indicating Rev1 can act in the bypass of minor groove lesions.

Consistent with our results and previous reports indicating PCNA interaction promotes the catalytic activity of Polκ [81, 82], we show that the PIP-boxes are important for TLS during ICL repair, indicating Polκ is recruited via PCNA. Interaction of Polκ with Rev1 is not essential for repair because mutation of Polκ's Rev1 interaction domain or depletion of Rev1 does not block TLS. The role of the UBZ domains of Polκ is less clear as their mutation only partially affects TLS during the repair of aldehyde ICLs by the FA pathway. A recent study also reported a partial defect in the bypass of minor groove single-strand lesions upon mutation of Polκ's UBZs [31]. Polκ's UBZs have been reported to interact with ubiquitylated PCNA during TLS to promote bypass [83]. While we detect PCNA ubiquitylation during ICL repair, in our primer extension experiments, Polκ's activity was not enhanced by interaction with PCNA-Ub. However, it has previously been reported that the activity of UBZ mutants in primer extension is only compromised when PCNA interaction via the PIP domain is limited [83]. Based on these data, we propose that the function of the UBZ domains is context-specific. They become important upon completion of PCNA interaction with other PIP box-containing proteins. This mechanism may promote polymerase switching [32, 84–87]. Another possibility we cannot rule out is that the UBZs bind other ubiquitylated proteins at the repair site, thereby contributing to TLS activity.

We also show a minor role for Rev1–Polζ in the insertion step of TLS during the repair of acetaldehyde- and acrolein-induced ICLs [19]. This role is independent of Polκ because Rev1-Polκ double depletion caused a more pronounced TLS defect compared to single Polκ depletion. Interestingly, the majority of the mutations introduced during the bypass of unhooked aldehyde ICLs are due to bypass activity promoted by Rev1–Polζ, while Polκ-mediated bypass is largely error-free (Fig. 5D and Supplementary Fig. S10C). Because Rev1's catalytic activity is limited to inserting cytosines [33, 82, 88], this would not result in mutations in our sequence context, indicating Rev1 likely promotes mutagenic bypass through a non-catalytic function. Consistently, Rev1 catalytic dead mutants generally do not affect mutagenic outcomes [89]. Therefore, other TLS polymerases that are recruited or otherwise promoted by Rev1 are likely to be involved.

Finally, even upon depletion of both Rev1 and Polκ, residual lesion bypass is still observed (Fig. 5B and C and Supplementary Fig. S9C–F), indicating that additional TLS polymerases can act on the unhooked aldehyde adducts. Candidates include Polη, previously suggested as the insertion polymerase for cisplatin ICL repair [90], or Polθ, which has some TLS capacity [91] and can bypass acrolein mono-adducts [77]. Both Polη and Polθ were detected on aldehyde ICL plasmids during repair in Mock, Rev1, and Polκ depleted extracts (Supplementary Fig. S10D). Another potential candidate would be Polδ, which has been suggested to promote TLS *in vitro* and *in vivo* [92–95].

Both Rev1–Polζ and Polκ also act in TLS during the repair of cisplatin ICLs but their role is different from aldehyde ICL repair. First, instead of in the insertion step, they act in the extension step of TLS. Second, the role of Polκ is independent of its catalytic activity but depends on interaction with Rev1. This is consistent with a recent study on the bypass of single-strand DNA lesions that, like cisplatin, affect the major groove of the DNA [31]. Furthermore, this study showed that the sensitivity of Polκ-deficient cells for cisplatin could be rescued by both WT and catalytically dead Polκ.

While our work has focused on the FA pathway branch of aldehyde ICL repair, it also provides insights into the mechanism of the excision-independent repair pathway. One interesting observation is that repair of the acetaldehyde and acrolein ICLs by the excision-independent pathway may have different requirements for TLS polymerases. The effect of Rev1 depletion on TLS of native acrolein ICLs was less extensive than on native acetaldehyde pICLs (Supplementary Fig. S4B), suggesting that TLS past these adducts involves different polymerases. While the acrolein and acetaldehyde ICLs only

differ by one methyl group, such subtle differences may play an important role in polymerase choice. This is in line with the difference in mutagenicity of acetaldehyde- and acrolein-monoadducts (Fig. 1H and [96]). We currently do not know the exact structure of the adduct generated by the incision-independent pathway, but based on our data, this may not be the mono-adduct precursor that generates the ICL. To gain further insight into this, it needs to be investigated which bond within the aldehyde ICL is cleaved during excision-independent ICL repair.

Because endogenous aldehyde ICLs have been reported to drive the FA phenotype [5–6, 9, 11, 97–98], it would be of interest to investigate whether Polκ deficiency can lead to FA. Genetic mouse models with combined deficiency in Polκ and Aldh2 or Adh5 could start to address this question. One complication could be that TLS polymerases are known to act redundantly, which may mitigate the severity of the observed defects. However, mutations in Rev7, a subunit of Polζ, were previously shown to cause FA [99–101], indicating defects in other TLS polymerases, including Polκ, could potentially also be involved in FA.

Our work shows that even in the same repair pathway, such as the FA pathway, different TLS polymerases act and have redundant functions. The choice of TLS polymerase seems to be determined by the structure of the adduct formed during repair. This knowledge is important to understand the mutagenic potential of ICL-inducing compounds and develop strategies to improve chemotherapeutic outcomes by inhibiting TLS polymerases.

Acknowledgements

We thank the members of the Knipscheer, Mattiroli, and Garaycoechea labs for discussions; Koichi Sato and Juan Garaycoechea for feedback on the manuscript; Robin van Schendel for advice in the mutation sequencing analysis; and The Hubrecht institute animal facility and caretakers for animal support.

Author contributions: Roxanne V. van der Sluijs (Conceptualization [equal], Formal analysis [lead], Investigation [lead], Methodology [equal], Validation [lead], Visualization [lead], Writing—original draft [equal], Writing—review & editing [equal]), Alexander E.E. Verkennis (Investigation [equal], Methodology [equal], Resources [equal], Validation [equal]), Michael R. Hodskinson (Conceptualization [equal], Data curation [equal], Methodology [equal], Resources [equal], Validation [equal], Writing—review & editing [equal]), Jamie Barnett (Data curation [equal], Formal analysis [equal], Investigation [equal], Methodology [equal], Writing—review & editing [equal]), Victoria M. Cruz (Formal analysis [equal]), Miguel Hernandez-Quiles (Investigation [supporting], Resources [equal]), Themistoklis Liolios (Investigation [supporting]), Sally B. Morton (Methodology [equal], Resources [equal]), Aiko Hendrikx (Investigation [supporting], Validation [supporting]), Collin Bos (Formal analysis [equal]), Harm Post (Investigation [supporting]), Chris Millington (Investigation [equal], Methodology [equal], Resources [equal], Visualization [supporting], Writing—review & editing [supporting]), Clément Rouillon (Methodology [supporting], Resources [equal], Writing—review & editing [equal]), Giulia Ricci (Investigation [equal], Resources [supporting]), Francesca Mattiroli (Supervision [equal], Writing—review & editing [equal]), David M. Williams (Methodology [equal], Resources [equal], Writing—review & editing [equal]), Maarten Altelaar (Supervision [equal]), and K.J. Patel (Conceptualization [equal]), Puck Knipscheer (Conceptualization [equal], Analysis [equal], Validation [equal], Writing—original draft [equal], Writing—review & editing [supporting], Supervision [equal], Funding acquisition [equal]), Michiel Vermeulen (Conceptualisation [equal], Supervision [equal]).

Supplementary data

Supplementary data is available at NAR online.

Conflict of interest

None declared.

Funding

This work was supported by the European Research Council (ERC) through an ERC consolidator grant ERC-CoG 101003210 (to P.K.), and an ERC starting grant ERC-StG 851564 (to F.M.); by the Netherlands Organization for Scientific Research (NWO) through the Gravitation program CancerGenomiCs.nl (to P.K.); The Oncode Institute, which is partly financed by The Dutch Cancer Society (KWF) (to P.K.). Funding to pay the Open Access publication charges for this article was provided by European Research Council (ERC).

Data availability

The mass spectrometry data generated using undepleted extract have been deposited to the ProteomeXchange Consortium via de PRIDE partner repository with the dataset identifier PXD062134. The mass spectrometry data generated using depleted extract have been deposited to the ProteomeXchange Consortium via de PRIDE partner repository with the dataset identifier PXD066315. The raw Illumina paired-end sequencing short-reads have been deposited to Zenodo and are accessible at https://doi.org/10.5281/zenodo.16362591.

References

1. Peake JD, Noguchi E. Fanconi anemia: current insights regarding epidemiology, cancer, and DNA repair. *Hum Genet* 2022;**141**:1811–36. https://doi.org/10.1007/s00439-022-02462-9
2. Peake JD, Noguchi C, Lin B *et al.* FANCD2 limits acetaldehyde-induced genomic instability during DNA replication in esophageal keratinocytes. *Mol Oncol* 2021;**15**:3109–24. https://doi.org/10.1002/1878-0261.13072
3. Auerbach AD. Fanconi anemia and its diagnosis. *Mutat Res* 2009;**668**:4–10. https://doi.org/10.1016/j.mrfmmm.2009.01.013
4. Niraj J, Färkkilä A, D'Andrea AD. The Fanconi anemia pathway in cancer. *Annu Rev Cancer Biol* 2019;**3**:457–78. https://doi.org/10.1146/annurev-cancerbio-030617-050422
5. Garaycoechea JI, Crossan GP, Langevin F *et al.* Genotoxic consequences of endogenous aldehydes on mouse haematopoietic stem cell function. *Nature* 2012;**489**:571–5. https://doi.org/10.1038/nature11368
6. Garaycoechea JI, Crossan GP, Langevin F *et al.* Alcohol and endogenous aldehydes damage chromosomes and mutate stem cells. *Nature* 2018;**553**:171–7. https://doi.org/10.1038/nature25154

7. Pontel LB, Rosado IV, Burgos-Barragan G *et al.* Endogenous formaldehyde is a hematopoietic stem cell genotoxin and metabolic carcinogen. *Mol Cell* 2015;**60**:177–88. https://doi.org/10.1016/j.molcel.2015.08.020
8. Oberbeck N, Langevin F, King G *et al.* Maternal aldehyde elimination during pregnancy preserves the fetal genome. *Mol Cell* 2014;**55**:807–17. https://doi.org/10.1016/j.molcel.2014.07.010
9. Langevin F, Crossan GP, Rosado IV *et al.* Fancd2 counteracts the toxic effects of naturally produced aldehydes in mice. *Nature* 2011;**475**:53–8. https://doi.org/10.1038/nature10192
10. Rosado IV, Langevin F, Crossan GP *et al.* Formaldehyde catabolism is essential in cells deficient for the Fanconi anemia DNA-repair pathway. *Nat Struct Mol Biol* 2011;**18**:1432–4. https://doi.org/10.1038/nsmb.2173
11. Wang M, Dingler FA, Patel KJ. Genotoxic aldehydes in the hematopoietic system. *Blood* 2022;**139**:2119–29. https://doi.org/10.1182/blood.2019004316
12. Dingler FA, Wang M, Mu A *et al.* Two aldehyde clearance systems are essential to prevent lethal formaldehyde accumulation in mice and humans. *Mol Cell* 2020;**80**:996–1012. https://doi.org/10.1016/j.molcel.2020.10.012
13. Klein Douwel D, Boonen RACM, Long DT *et al.* XPF–ERCC1 acts in unhooking DNA interstrand crosslinks in cooperation with FANCD2 and FANCP/SLX4. *Mol Cell* 2014;**54**:460–71. https://doi.org/10.1016/j.molcel.2014.03.015
14. Räschle M, Knipsheer P, Enoiu M *et al.* Mechanism of replication-coupled DNA interstrand crosslink repair. *Cell* 2008;**134**:969–80. https://doi.org/10.1016/j.cell.2008.08.030
15. Knipscheer P, Räschle M, Smogorzewska A *et al.* The Fanconi anemia pathway promotes replication-dependent DNA interstrand cross-link repair. *Science* 2009;**326**:1698–701. https://doi.org/10.1126/science.1182372
16. Long DT, Räschle M, Joukov V *et al.* Mechanism of RAD51-dependent DNA interstrand cross-link repair. *Science* 2011;**333**:84–7. https://doi.org/10.1126/science.1204258
17. Budzowska M, Graham TG, Sobeck A *et al.* Regulation of the Rev1–pol ζ complex during bypass of a DNA interstrand cross-link. *EMBO J* 2015;**34**:1971–85. https://doi.org/10.15252/embj.201490878
18. Michl J, Zimmer J, Tarsounas M. Interplay between Fanconi anemia and homologous recombination pathways in genome integrity. *EMBO J* 2016;**35**:909–23. https://doi.org/10.15252/embj.201693860
19. Hodskinson MR, Bolner A, Sato K *et al.* Alcohol-derived DNA crosslinks are repaired by two distinct mechanisms. *Nature* 2020;**579**:603–8. https://doi.org/10.1038/s41586-020-2059-5
20. Kozekov ID, Nechev LV, Sanchez A *et al.* Interchain cross-linking of DNA mediated by the principal adduct of acrolein. *Chem Res Toxicol* 2001;**14**:1482–5. https://doi.org/10.1021/tx010127h
21. Minko IG, Kozekov ID, Harris TM *et al.* Chemistry and biology of DNA containing 1,N^2-deoxyguanosine adducts of the α,β-unsaturated aldehydes acrolein, crotonaldehyde, and 4-hydroxynonenal. *Chem Res Toxicol* 2009;**22**:759–78. https://doi.org/10.1021/tx9000489
22. Stone MP, Cho YJ, Huang H *et al.* Interstrand DNA cross-links induced by α,β-unsaturated aldehydes derived from lipid peroxidation and environmental sources. *Acc Chem Res* 2008;**41**:793–804. https://doi.org/10.1021/ar700246x
23. Sanchez AM, Kozekov ID, Harris TM *et al.* Formation of inter- and intrastrand imine type DNA–DNA cross-links through secondary reactions of aldehydic adducts. *Chem Res Toxicol* 2005;**18**:1683–90. https://doi.org/10.1021/tx0500528
24. Voordeckers K, Colding C, Grasso L *et al.* Ethanol exposure increases mutation rate through error-prone polymerases. *Nat Commun* 2020;**11**:3664. https://doi.org/10.1038/s41467-020-17447-3
25. Jung M, Ilyashov I, Park Y *et al.* ALDH9A1 deficiency as a source of endogenous DNA damage that requires repair by the Fanconi anemia pathway. *J Cell Biol* 2025;**224**:e202407141. https://doi.org/10.1083/jcb.202407141
26. Moghe A, Ghare S, Lamoreau B *et al.* Molecular mechanisms of acrolein toxicity: relevance to human disease. *Toxicol Sci* 2015;**143**:242–55. https://doi.org/10.1093/toxsci/kfu233
27. Stevens JF, Maier CS. Acrolein: sources, metabolism, and biomolecular interactions relevant to human health and disease. *Mol Nutr Food Res* 2008;**52**:7–25. https://doi.org/10.1002/mnfr.200700412
28. Roy U, Schärer OD. Involvement of translesion synthesis DNA polymerases in DNA interstrand crosslink repair. *DNA Repair (Amst)* 2016;**44**:33–41. https://doi.org/10.1016/j.dnarep.2016.05.004
29. Bezalel-Buch R, Cheun YK, Roy U *et al.* Bypass of DNA interstrand crosslinks by a Rev1–DNA polymerase ζ complex. *Nucleic Acids Res* 2020;**48**:8461–73. https://doi.org/10.1093/nar/gkaa580
30. Ho TV, Schärer OD. Translesion DNA synthesis polymerases in DNA interstrand crosslink repair. *Environ Mol Mutagen* 2010;**51**:552–66. https://doi.org/10.1002/em.20573
31. Sellés-Baiget S, Ambjørn SM, Carli A *et al.* Catalytic and noncatalytic functions of DNA polymerase κ in translesion DNA synthesis. *Nat Struct Mol Biol* 2025;**32**:300–14. https://doi.org/10.1038/s41594-024-01395-3
32. Lehmann AR, Niimi A, Ogi T *et al.* Translesion synthesis: Y-family polymerases and the polymerase switch. *DNA Repair (Amst)* 2007;**6**:891–9. https://doi.org/10.1016/j.dnarep.2007.02.003
33. Guo C, Kosarek-Stancel JN, Tang TS *et al.* Y-family DNA polymerases in mammalian cells. *Cell Mol Life Sci* 2009;**66**:2363–81. https://doi.org/10.1007/s00018-009-0024-4
34. Ohashi E, Murakumo Y, Kanjo N *et al.* Interaction of hREV1 with three human Y-family DNA polymerases. *Genes Cells* 2004;**9**:523–31. https://doi.org/10.1111/j.1356-9597.2004.00747.x
35. Sale JE, Lehmann AR, Woodgate R. Y-family DNA polymerases and their role in tolerance of cellular DNA damage. *Nat Rev Mol Cell Biol* 2012;**13**:141–52. https://doi.org/10.1038/nrm3289
36. Gallina I, Hendriks IA, Hoffmann S *et al.* The ubiquitin ligase RFWD3 is required for translesion DNA synthesis. *Mol Cell* 2021;**81**:442–58. https://doi.org/10.1016/j.molcel.2020.11.029
37. Kanao R, Kawai H, Taniguchi T *et al.* RFWD3 and translesion DNA polymerases contribute to PCNA modification-dependent DNA damage tolerance. *Life Sci Alliance* 2022;**5**:e202201584. https://doi.org/10.26508/lsa.202201584
38. Feeney L, Muñoz IM, Lachaud C *et al.* RPA-mediated recruitment of the E3 ligase RFWD3 is vital for interstrand crosslink repair and human health. *Mol Cell* 2017;**66**:610–21. https://doi.org/10.1016/j.molcel.2017.04.021
39. Wang Z, Huang M, Ma X *et al.* REV1 promotes PCNA monoubiquitylation through interacting with ubiquitylated RAD18. *J Cell Sci* 2016;**129**:1223–33. https://doi.org/10.1242/jcs.179408
40. Keaton MA, Dutta A. Rad18 emerges as a critical regulator of the Fanconi anemia pathway. *Cell Cycle* 2011;**10**:24142415 https://doi.org/10.4161/cc.10.15.15930
41. Yang Y, Gao Y, Zlatanou A *et al.* Diverse roles of RAD18 and Y-family DNA polymerases in tumorigenesis. *Cell Cycle* 2018;**17**:833–43. https://doi.org/10.1080/15384101.2018.1456296
42. Masuda Y, Kanao R, Kaji K *et al.* Different types of interaction between PCNA and PIP boxes contribute to distinct cellular functions of Y-family DNA polymerases. *Nucleic Acids Res* 2015;**43**:7898–910. https://doi.org/10.1093/nar/gkv712
43. Ogi T, Kannouche P, Lehmann AR. Localisation of human Y-family DNA polymerase κ: relationship to PCNA foci. *J Cell Sci* 2005;**118**:129–36. https://doi.org/10.1242/jcs.01603
44. Minko IG, Harbut MB, Kozekov ID *et al.* Role for DNA polymerase kappa in the processing of N^2-N^2-guanine

interstrand cross-links. *J Biol Chem* 2008;**283**:17075–82. https://doi.org/10.1074/jbc.m801238200
45. Lior-Hoffmann L, Ding S, Geacintov NE *et al.* Structural and dynamic characterization of polymerase κ's minor groove lesion processing reveals how adduct topology impacts fidelity. *Biochemistry* 2014;**53**:5683–91. https://doi.org/10.1021/bi5007964
46. Minko IG, Yamanaka K, Kozekov ID *et al.* Replication bypass of the acrolein-mediated deoxyguanine DNA-peptide cross-links by DNA polymerases of the DinB family. *Chem Res Toxicol* 2008;**21**:1983–90. https://doi.org/10.1021/tx800174a
47. Gerlach VL, Feaver WJ, Fischhaber PL *et al.* Purification and characterization of polκ, a DNA polymerase encoded by the human DINB1 gene. *J Biol Chem* 2001;**276**:92–8. https://doi.org/10.1074/jbc.M004413200
48. Morton SB, Finger LD, van der Sluijs R *et al.* Efficient synthesis of DNA duplexes containing reduced acetaldehyde interstrand cross-links. *J Am Chem Soc* 2023;**145**:953–9. https://doi.org/10.1021/jacs.2c10070
49. Enoiu M, Ho TV, Long DT *et al.* Construction of plasmids containing site-specific DNA interstrand cross-links for biochemical and cell biological studies. *Methods Mol Biol* 2012;**920**:203–19. https://doi.org/10.1007/978-1-61779-998-3_15
50. Zhang J, Dewar JM, Budzowska M *et al.* DNA interstrand cross-link repair requires replication-fork convergence. *Nat Struct Mol Biol* 2015;**22**:242–7. https://doi.org/10.1038/nsmb.2956
51. Semlow DR, Zhang J, Budzowska M *et al.* Replication-dependent unhooking of DNA interstrand cross-links by the NEIL3 glycosylase. *Cell* 2016;**167**:498–511. https://doi.org/10.1016/j.cell.2016.09.008
52. Lebofsky R, Takahashi T, Walter JC. DNA replication in nucleus-free *Xenopus* egg extracts. *Methods Mol Biol* 2009;**521**:229–52. https://doi.org/10.1007/978-1-60327-815-7_3
53. Sparks J, Walter JC. Extracts for analysis of DNA replication in a nucleus-free system. *Cold Spring Harb Protoc* 2019;**2019**:194–206. https://doi.org/10.1101/pdb.prot097154
54. Klein Douwel D, Hoogenboom WS, Boonen RA *et al.* Recruitment and positioning determine the specific role of the XPF–ERCC1 endonuclease in interstrand crosslink repair. *EMBO J* 2017;**36**:2034–46. https://doi.org/10.15252/embj.201695223
55. Girardot C, Scholtalbers J, Sauer S *et al.* Je, a versatile suite to handle multiplexed NGS libraries with unique molecular identifiers. *BMC Bioinformatics* 2016;**17**:4–9. https://doi.org/10.1186/s12859-016-1284-2
56. Smith T, Heger A, Sudbery I. UMI-tools: modeling sequencing errors in Unique Molecular Identifiers to improve quantification accuracy. *Genome Res* 2017;**27**:491–9. https://doi.org/10.1101/gr.209601.116
57. Md V, Misra S, Li H *et al.* Efficient architecture-aware acceleration of BWA-MEM for multicore systems. In: *Proceedings - 2019 IEEE 33rd International Parallel and Distributed Processing Symposium, IPDPS*. Rio de Janeiro, Brazil: 2019, 314–24. https://doi.org/10.1109/IPDPS.2019.00041
58. van Schendel R, Schimmel J, Tijsterman M. SIQ: easy quantitative measurement of mutation profiles in sequencing data. *NAR Genom Bioinform* 2022;**4**:lqac063. https://doi.org/10.1093/nargab/lqac063
59. Larsen NB, Gao AO, Sparks JL *et al.* Replication-coupled DNA–protein crosslink repair by SPRTN and the proteasome in *Xenopus* egg extracts. *Mol Cell* 2019;**73**:574–88. https://doi.org/10.1016/j.molcel.2018.11.024
60. Cox J, Mann M. MaxQuant enables high peptide identification rates, individualized p.p.b.-range mass accuracies and proteome-wide protein quantification. *Nat Biotechnol* 2008;**26**:1367–72. https://doi.org/10.1038/nbt.1511
61. Temu T, Mann M, Räschle M *et al.* Homology-driven assembly of NOn-redundant protEin sequence sets (NOmESS) for mass spectrometry. *Bioinformatics* 2016;**32**:1417–9. https://doi.org/10.1093/bioinformatics/btv756
62. Demichev V, Messner CB, Vernardis SI *et al.* DIA-NN: neural networks and interference correction enable deep proteome coverage in high throughput. *Nat Methods* 2020;**17**:41–4. https://doi.org/10.1038/s41592-019-0638-x
63. Dharadhar S, van Dijk WJ, Scheffers S *et al.* Insert L1 is a central hub for allosteric regulation of USP1 activity. *EMBO Rep* 2021;**22**:e51749. https://doi.org/10.15252/embr.202051749
64. Rouillon C, Eckhardt BV, Kollenstart L *et al.* CAF-1 deposits newly synthesized histones during DNA replication using distinct mechanisms on the leading and lagging strands. *Nucleic Acids Res* 2023;**51**:3770–92. https://doi.org/10.1093/nar/gkad171
65. Huang H, Wang H, Kozekova A *et al.* Formation of a N^2-dG:N^2-dG carbinolamine DNA cross-link by the *trans*-4-hydroxynonenal-derived (6*S*,8R,11*S*) 1,N^2-dG adduct. *J Am Chem Soc* 2011;**133**:16101–10. https://doi.org/10.1021/ja205145q
66. Kozekov ID, Nechev LV, Moseley MS *et al.* DNA interchain cross-links formed by acrolein and crotonaldehyde. *J Am Chem Soc* 2003;**125**:50–61. https://doi.org/10.1021/ja020778f
67. Housh K, Jha JS, Haldar T *et al.* Formation and repair of unavoidable, endogenous interstrand cross-links in cellular DNA. *DNA Repair (Amst)* 2021;**98**:103029. https://doi.org/10.1016/j.dnarep.2020.103029
68. Wu RA, Semlow DR, Kamimae-Lanning AN *et al.* TRAIP is a master regulator of DNA interstrand crosslink repair. *Nature* 2019;**567**:267–72. https://doi.org/10.1038/s41586-019-1002-0
69. Stern HR, Sefcikova J, Chaparro VE *et al.* Mammalian DNA polymerase kappa activity and specificity. *Molecules* 2019;**24**:2805 9–17. https://doi.org/10.3390/molecules24152805
70. Takeiri A, Wada NA, Motoyama S *et al. In vivo* evidence that DNA polymerase kappa is responsible for error-free bypass across DNA cross-links induced by mitomycin C. *DNA Repair (Amst)* 2014;**24**:113–21. https://doi.org/10.1016/j.dnarep.2014.09.002
71. Williams HL, Gottesman ME, Gautier J. Replication-independent repair of DNA interstrand crosslinks. *Mol Cell* 2012;**47**:140–7. https://doi.org/10.1016/j.molcel.2012.05.001
72. Guo C, Tang TS, Bienko M *et al.* Requirements for the interaction of mouse Polκ with ubiquitin and its biological significance. *J Biol Chem* 2008;**283**:4658–64. https://doi.org/10.1074/jbc.M709275200
73. Ohashi E, Hanafusa T, Kamei K *et al.* Identification of a novel REV1-interacting motif necessary for DNA polymerase κ function. *Genes Cells* 2009;**14**:101–11. https://doi.org/10.1111/j.1365-2443.2008.01255.x
74. Hishiki A, Hashimoto H, Hanafusa T *et al.* Structural basis for novel interactions between human translesion synthesis polymerases and proliferating cell nuclear antigen. *J Biol Chem* 2009;**284**:10552–60. https://doi.org/10.1074/jbc.M809745200
75. Haracska L, Unk I, Johnson RE *et al.* Stimulation of DNA synthesis activity of human DNA polymerase κ by PCNA. *Mol Cell Biol* 2002;**22**:784–91. https://doi.org/10.1128/MCB.22.3.784-791.2002
76. Lone S, Townson SA, Uljon SN *et al.* Human DNA polymerase κ encircles DNA: implications for mismatch extension and lesion bypass. *Mol Cell* 2007;**25**:601–14. https://doi.org/10.1016/j.molcel.2007.01.018
77. Yoon JH, Hodge RP, Hackfeld LC *et al.* Genetic control of predominantly error-free replication through an acrolein-derived minor-groove DNA adduct. *J Biol Chem* 2018;**293**:2949–58. https://doi.org/10.1074/jbc.RA117.000962
78. Choi JY, Angel KC, Guengerich FP. Translesion synthesis across bulky N^2-alkyl guanine DNA adducts by human DNA

polymerase κ. *J Biol Chem* 2006;**281**:21062–72. https://doi.org/10.1074/jbc.M602246200
79. Takenaka K, Ogi T, Okada T *et al.* Involvement of vertebrate Polκ in translesion DNA synthesis across DNA monoalkylation damage. *J Biol Chem* 2006;**281**:2000–4. https://doi.org/10.1074/jbc.M506153200
80. Temviriyanukul P, Meijers M, Van Hees-Stuivenberg S *et al.* Different sets of translesion synthesis DNA polymerases protect from genome instability induced by distinct food-derived genotoxins. *Toxicol Sci* 2012;**127**:130–8. https://doi.org/10.1093/toxsci/kfs074
81. Guo C, Fischhaber PL, Luk-Paszyc MJ *et al.* Mouse Rev1 protein interacts with multiple DNA polymerases involved in translesion DNA synthesis. *EMBO J* 2003;**22**:6621–30. https://doi.org/10.1093/emboj/cdg626
82. Guo C, Sonoda E, Tang TS *et al.* REV1 protein interacts with PCNA: significance of the REV1 BRCT domain *in vitro* and *in vivo*. *Mol Cell* 2006;**23**:265–71. https://doi.org/10.1016/j.molcel.2006.05.038
83. Lancey C, Tehseen M, Bakshi S *et al.* Cryo-EM structure of human pol κ bound to DNA and mono-ubiquitylated PCNA. *Nat Commun* 2021;**12**:6095. https://doi.org/10.1038/s41467-021-26251-6
84. Zhao L, Washington MT. Translesion synthesis: insights into the selection and switching of DNA polymerases. *Genes* 2017;**8**:1–25. https://doi.org/10.3390/genes8010024
85. Plosky BS, Woodgate R. Switching from high-fidelity replicases to low-fidelity lesion-bypass polymerases. *Curr Opin Genet Dev* 2004;**14**:113–9. https://doi.org/10.1016/j.gde.2004.02.002
86. Kannouche PL, Lehmann AR. Ubiquitination of PCNA and the polymerase switch in human cells. *Cell Cycle* 2004;**3**:1009–11. https://doi.org/10.4161/cc.3.8.1074
87. Zhang Z, Zhang S, Lin SHS *et al.* Structure of monoubiquitinated PCNA: implications for DNA polymerase switching and Okazaki fragment maturation. *Cell Cycle* 2012;**11**:2128–36. https://doi.org/10.4161/cc.20595
88. Ma X, Tang TS, Guo C. Regulation of translesion DNA synthesis in mammalian cells. *Environ Mol Mutagen* 2020;**61**:680–92. https://doi.org/10.1002/em.22359
89. Ross AL, Simpson LJ, Sale JE. Vertebrate DNA damage tolerance requires the C-terminus but not BRCT or transferase domains of REV1. *Nucleic Acids Res* 2005;**33**:1280–9. https://doi.org/10.1093/nar/gki279
90. Ummat A, Rechkoblit O, Jain R *et al.* Structural basis for cisplatin DNA damage tolerance by human polymerase η during cancer chemotherapy. *Nat Struct Mol Biol* 2012;**19**:628–32. https://doi.org/10.1038/nsmb.2295
91. Yoon JH, Johnson RE, Prakash L *et al.* DNA polymerase θ accomplishes translesion synthesis opposite 1, N^6-ethenodeoxyadenosine with a remarkably high fidelity in human cells. *Genes Dev* 2019;**33**:282–7. https://doi.org/10.1101/gad.320531.118
92. Hirota K, Tsuda M, Mohiuddin *et al. In vivo* evidence for translesion synthesis by the replicative DNA polymerase δ. *Nucleic Acids Res* 2016;**44**:7242–50. https://doi.org/10.1093/nar/gkw439
93. Hirota K, Yoshikiyo K, Guilbaud G *et al.* The POLD3 subunit of DNA polymerase δ can promote translesion synthesis independently of DNA polymerase ζ. *Nucleic Acids Res* 2015;**43**:1671–83. https://doi.org/10.1093/nar/gkv023
94. Dieckman LM, Washington MT. PCNA trimer instability inhibits translesion synthesis by DNA polymerase η and by DNA polymerase δ. *DNA Repair (Amst)* 2013;**12**:367–76. https://doi.org/10.1016/j.dnarep.2013.02.007
95. Choi JY, Lim S, Kim EJ *et al.* Translesion synthesis across abasic lesions by human B-Family and Y-Family DNA polymerases α, δ, η, ι, κ, and REV1. *J Mol Biol* 2010;**404**:34–44. https://doi.org/10.1016/j.jmb.2010.09.015
96. Vijayraghavan S, Saini N. Aldehyde-associated mutagenesiscurrent state of knowledge. *Chem Res Toxicol* 2023;**36**:983–1001. https://doi.org/10.1021/acs.chemrestox.3c00045
97. Mu A, Hira A, Niwa A *et al.* Analysis of disease model iPSCs derived from patients with a novel Fanconi anemia–like IBMFS ADH5/ALDH2 deficiency. *Blood* 2021;**137**:2021–32. https://doi.org/10.1182/blood.2020009111
98. Mu A, Hira A, Mori M *et al.* Fanconi anemia and Aldehyde Degradation Deficiency Syndrome: metabolism and DNA repair protect the genome and hematopoiesis from endogenous DNA damage. *DNA Repair (Amst)* 2023;**130**:103546. https://doi.org/10.1016/j.dnarep.2023.103546
99. Bluteau D, Masliah-Planchon J, Clairmont C *et al.* Biallelic inactivation of REV7 is associated with Fanconi anemia. *J Clin Invest* 2016;**126**:3580–4. https://doi.org/10.1172/JCI88010
100. Maggs LR, McVey M. REV7: a small but mighty regulator of genome maintenance and cancer development. *Front Oncol* 2024;**14**:1516165. https://doi.org/10.3389/fonc.2024.1516165
101. Murakumo Y, Sakurai Y, Kato T *et al.* REV7 in cancer biology and management. *Cancers (Basel)* 2023;**15**:1721. https://doi.org/10.3390/cancers15061721

Received: March 31, 2025. **Revised:** July 26, 2025. **Accepted:** July 30, 2025